Vertical distribution of sources and sinks of VOCs within a boreal forest canopy

Ross Petersen[1], Thomas Holst[1], Meelis Mölder[1], Natascha Kljun[2], and Janne Rinne[1, 3]

[1]Department of Physical Geography and Ecosystem Science, Lund University, Lund, Sweden
[2]Centre for Environmental and Climate Science, Lund University, Lund, Sweden.
[3]Natural Resources Institute Finland (Luke), Helsinki, Finland

Correspondence to: Thomas Holst (thomas.holst@nateko.lu.se)

Abstract. The ecosystem-atmosphere flux of biogenic volatile organic compounds (BVOCs) has important impacts on tropospheric oxidative capacity and the formation of secondary organic aerosols, influencing air quality and climate. Here we present within-canopy measurements of a set of dominant BVOCs in a managed spruce- and pine-dominated boreal forest located at the ICOS station Norunda in Sweden, collected using proton transfer reaction mass spectrometry (PTR-MS) during 2014-2016, and vertical emission profiles derived from these data. Ozone concentrations were simultaneously measured in conjunction with these PTR-MS measurements. The main BVOCs investigated with the PTR-MS were isoprene, monoterpenes, methanol, acetaldehyde, and acetone. The distribution of BVOC sources and sinks in the forest canopy was explored using Lagrangian dispersion matrix methods, in particular continuous near-field theory. The forest canopy was found to contribute ca. 86% to the total monoterpene emission in summertime, whereas the below-canopy and canopy emission was comparable (ca. 42% and 58% respectively) during the autumn period. This result indicates that boreal forest litter and other below-canopy emitters are a ~~principle~~principal source for total forest monoterpene emissions during autumn months. During night, our results for methanol, acetone, and acetaldehyde seasonally present strong sinks in the forest canopy, especially in the autumn, likely due to the nighttime formation of dew on vegetation surfaces.

1 Introduction

Terrestrial emission of volatile organic compounds (VOCs) has a significant global impact on atmospheric chemistry, biogenic VOC (BVOC) emissions being the globally most important source of reactive organic compounds into the atmosphere (Seinfeld and Pandis, 2016). Particularly in remote and rural forested areas, the BVOC emissions tend to dominate over anthropogenic VOC sources (Simpson et al., 1999; Lindfors and Laurila, 2000).

BVOCs have a significant role in the production and lifetime of tropospheric ozone (Chameides et al., 1992) and impact on the lifetimes of methane (Collins et al., 2002). In addition, BVOCs serve as a major precursor source for the formation and growth of organic aerosols (e.g., Andreae and Crutzen, 1997). Oxygenated VOC compounds, such as acetone, can also

modify hydroxyl radical concentrations in the upper troposphere (Fehsenfeld et al., 1992; Mckeen et al., 1997), and/or contribute to the formation of peroxyacetic nitric anhydride (PAN) compounds that can act as a reservoir for nitrogen oxides (NOx) (Roberts et al., 2002). Methanol is the most abundant non-methane volatile organic compound in the troposphere (e.g., Jacob et al 2004), and it is a significant atmospheric source of formaldehyde (Riemer et al., 1998; Palmer et al., 2003)
35 and CO (Duncan et al., 2004) in global chemistry budgets.

Boreal forests are a major source of BVOCs in the atmosphere (Guenther et al. 1995), with emissions dominated by monoterpenes. While boreal zone vegetation on average tend to have lower emission rates than forests in warmer biomes, due to the cooler boreal climate and lower biomass density, the large areal coverage of boreal forest as a terrestrial forest
40 biome (ca. 27% of global forest area) (FAO 2020) makes it an important VOC source.

The seasonality of boreal BVOC emissions (Aalto et al., 2014; Hakola et al., 2017; Wang et al., 2017), as well as seasonal changes in the vertical disposition of BVOC sources and sinks in the forest canopy, is of importance to long-term BVOC emissions from boreal forests. For de novo emissions, it is well known that the rate of isoprene and terpenoid production is
45 PAR- and leaf temperature-dependent (e.g., Arneth et al., 2011; Ghirardo et al., 2010; Guenther et al., 1995; Guenther et al., 1993). Emission from specialized internal storage structures such as resin ducts, a common and frequently dominant feature of monoterpene emission from coniferous plants, is typically modeled as a function of leaf temperature (e.g., Guenther et al., 1995; Guenther et al., 1993; Schurgers et al., 2009; Tingey et al., 1980). In addition to the seasonality of PAR and leaf temperature, there are strong interactions between seasonality and underlying biological drivers of BVOC emission,
50 including individual plant phenology, forest biomass growth and senescence, in addition to species-specific emission characteristics (Niinemets and Monson, 2013). There is also the role of biotic and abiotic stresses in heterogeneous emission patterns (e.g., Amin et al., 2012; Loreto and Schnitzler, 2010; Niinemets, 2010; Schade and Goldstein, 2003). Meteorological and soil water conditions can have a significant impact on methanol, acetaldehyde, and acetone exchange (e.g., Kreuzwieser et al., 2000). In terms of sinks, methanol and other water-soluble VOCs can be taken up by liquid water
55 present on forest canopy surfaces (Karl et al., 2004). Dry uptake of BVOCs by forest canopy biomass is another consideration (e.g., Karl et al., 2004). Monoterpene uptake by leaf surfaces of non-emitting deciduous tree species under high ambient concentrations can lead to altered behavior of total monoterpene fluxes leaving the forest canopy (e.g., Copolovici and Niinemets, 2005; Noe et al., 2007). Forming a clear understanding of these processes occurring in boreal forest canopy at a seasonal-scale is important for improved BVOC emission and climate modeling (Aalto et al., 2014; Rinne
60 et al., 2009; Seco et al., 2007; Tarvainen et al., 2007).

While net BVOC emissions from boreal forests have been investigated extensively in previous studies (e.g., Aalto et al., 2014; Rantala et al., 2015; Rinne et al., 2007; Taipale et al., 2011), the number of studies regarding the vertical distribution of BVOC sources and sinks in the forest canopy are far more sparse (e.g., Karl et al., 2004). As the emission of VOCs from

65 plants can vary from leaf to leaf and between individuals of the same species (Bäck et al., 2012; Hakola et al., 2017), it is challenging to use only leaf- and branch--level measurements to interpret exchange processes, often requiring that investigations of in-canopy sources and sinks rely on modeling exchange processes (e.g., Zhou et al., 2017). The quantification of BVOC exchange processes in boreal forests at a full ecosystem-level necessitates that an evaluation be based at least in part on micrometeorological techniques and whole-canopy measurements.

70

Here we present measurements of BVOCs from a managed coniferous boreal forest located at the ICOS (Integrated Carbon Observation System) station Norunda in Sweden, collected at several heights throughout the canopy using proton transfer reaction mass spectrometry (PTR-MS). We aim to resolve the sink and source distribution of BVOCs within the forest canopy using Lagrangian dispersion theory (Warland and Thurtell, 2000).

75 **2 Methods**

2.1 Site description

The study site, ICOS research station Norunda (SE-Nor; www.icos-sweden.se/norunda), is located at 60°05′N, 17°29′E, approximately 30 km north of Uppsala, Sweden. The station is surrounded by a mixed-conifer forest of Scots pine (*Pinus sylvestris*) and Norway spruce (*Picea abies*). This forest was between 80 and 110 years old at the time of campaign
80 measurements in 2014-2016 (e.g., Lagergren et al., 2005; Lundin et al., 1999), and the forest canopy height was 28m (Wang et al., 2017). The area has been managed forest for approximately the last 200 years. The flux measurement station at Norunda has operated since 1994, measuring forest-atmosphere CO_2 exchange, and is now a class 1 and 2 ICOS atmosphere and ecosystem station, respectively. The station is equipped with a 102 m tower for flux and atmospheric measurements (Lindroth et al., 1998; Lundin et al., 1999). A station map is shown in Figure 1, the average flux footprint (displayed in
85 Figure 1) at 36 m on the station flux tower for the 2014 – 2016 campaign period was calculated using the flux footprint model developed by Kljun et al. (2015). There is a small fraction (<5%) of deciduous trees within 500 m of the station tower, primarily birch (*Betula sp.*). The dominant understory vegetation at the station is bilberry (*Vaccinium myrtillus*) and lingonberry (*Vaccinium vitis-idaea*), in addition to several species of dwarf-shrubs, ferns, and grasses. The bottom layer vegetation predominantly consists of a thick layer of feather moss (*Pleurozium schreberi* and *Hylocomium splendens*). From
90 2009 to 2014, the leaf area index of the Norunda forest in proximity of the tower was determined to be approximately 3.6 ($\pm$0.4) m^2 m^{-2} using a LAI 2000 (Li-Cor Inc., Lincoln, USA). During the 25 years prior to 2014, the mean annual temperature was 6.4°C and the mean annual precipitation was 531 mm as measured at the station. The growing season, defined as daily air temperatures above 5 °C, is typically from May to September. New needle growth typically begins in April. Foliation of deciduous trees and plants usually occurs in May and senescence in October (+- 15 days).

95
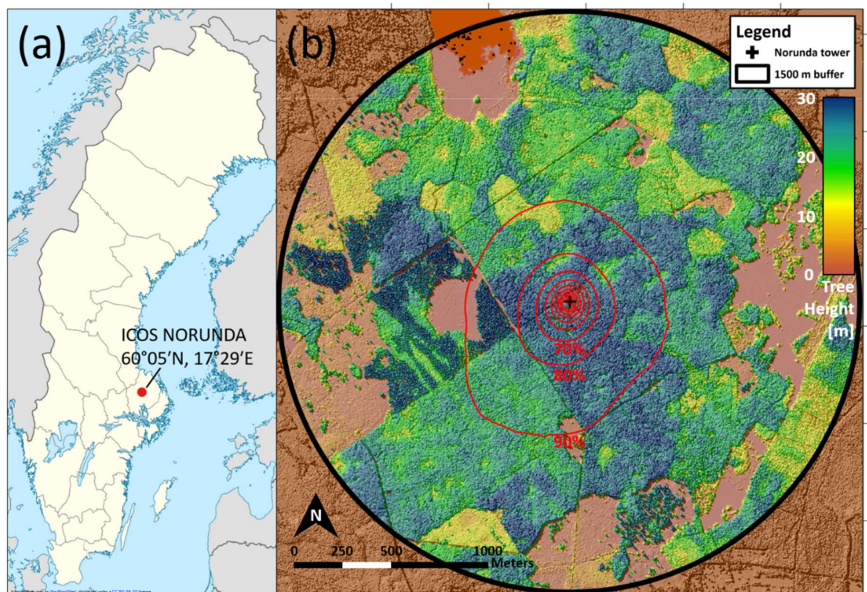
Figure 1: Location of ICOS station Norunda a) relative to Sweden as a whole. b) shows the tree height surrounding the station in detail from above (2011) and the footprint of the Norunda tower at 36 m (red contours) for the 2014 – 2016 campaign period. Contours were calculated using the FFP footprint model (Kljun et al., 2015). Each contour line adds 10% contribution (contours
100   **show 10% to 90%). Black cross is tower location.**

In addition to the typical ICOS station standard instrumentation (Rebmann et al., 2018)(cite, description of general layout), there are eleven Metek 3D sonic anemometers (USA-1, Metek GmbH, Germany) mounted on the flux tower at heights from 4 to 100.5 m above ground level (see Figure 2). These anemometers are mounted on booms extending 5 m towards north-

105   northwest from the tower.

2.2 Trace gas sampling

Ambient air from six heights (4, 8.5, 13.5, 19, 24.5, and 33.5 m a.g.l.; forest canopy height H=28m)– was pulled down by two vacuum pumps (Vaccubrand ME2, Wertheim, Germany) using six heated and insulated PFA Teflon tubes mounted on the station flux tower (Figure 2). These sampling tubes were each 45 m of length with OD of 3/8". The flow rate through

110   each PFA tube was 20 L/min. Sample air residence time in tower tubing before reaching instrumentation was ca. 4.5 s. The measurements took place during several periods from 2014 to 2016, and were collected by sampling at each height for 5 minutes consecutively during a 30-minute sampling cycle. BVOC measurements were collected from 12 September 2014 to

11 January 2015, 21 May 2015 to 16 December 2015, and 28 April 2016 to 5 July 2016. Ozone measurements were collected using the same sampling cycle from 13 September 2014 to 10 October 2016. A Campbell Scientific (Logan, UT, USA) CR1000 datalogger with SDM-CD8S switch module was used to control a set of PTFE-coated solenoid valves (Parker Hannifin, Hollis, NH, USA) to subsample air (total 1 L min^{-1}) from the selected main inlet flow for trace gas analysis.
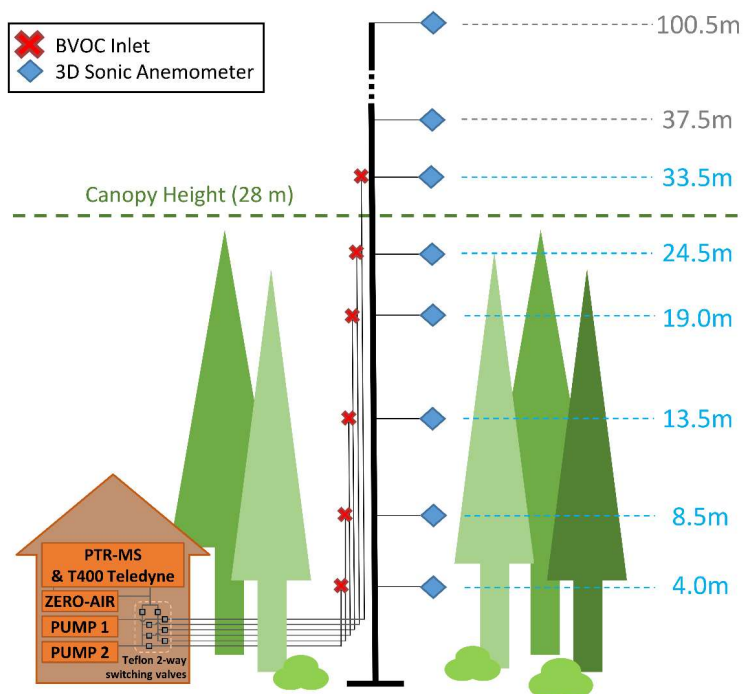
Figure 2: BVOC inlet setup at Norunda. Shown are the heights of the 3D sonic anemometers (blue diamond) and BVOC inlets (red cross) at the station flux tower. The canopy top height is at approximately 28 m. Instrument shed contained the PTR-MS, the Model T400 Teledyne ozone analyzer, zero-air generator for the PTR-MS, PTFE valve switching system and pair of vacuum pumps for pulling air through the tower inlet tubing. Two pumps are were used to pull air through the tower inlets. Switching every 5 minutes, pump #1 services levels 1, 3, and 5 (33.5, 19, and 8.5 m), while pump #2 services levels 2, 4, 6 (24.5, 13.5, and 4 m). The tower inlet tubes from which sample air wasis being actively drawn for sampling wasis therefore pumped while the tower line for the next 5-minute period of the 30-minute cycle wasis pre-pumped.

2.3 Trace gas analysis

Part (0.3 L min^{-1}) of the air subsample flow was analyzed for BVOCs using a Proton Transfer Reaction - quadrupole Mass Spectrometer (HS-PTR-MS, Ionicon Analytik, Innsbruck, Austria). The PTR-MS uses the protonation of compounds by H$_3$O$^+$ ions in a drift tube to ionize the target compounds, with subsequent detection by a mass spectrometer. Compound concentrations were determined using a primary ion H$_3$O$^+$ (m/z 21+) and target ion count rate along with other instrumental parameters following Lindinger et al. (1998) and Holst et al. (2010). For these measurements, the drift tube pressure was set to 2.2 mbar and drift tube temperature was maintained at 60°C (E/N=130 Td). The ozone concentrations were measured from the remaining subsample flow (0.7 L min^{-1}) using a UV absorption analyzer (Model T400, Teledyne API, San Diego, CA, USA) in parallel to the BVOC measurements. Reference measurements to determine the instrumental background of the PTR-MS were periodically performed by passing sample air through a heated catalytic converter (Zero Air Generator model 75-83, Parker Balston, Haverhill, MA, USA). Readings of the PTR-MS count rate for target ions were corrected for the mean daily zero-air background values normalized to the count rate of the primary ion 21+ during analysis. During concentration profile analysis, the first and last minute of each 5-minute level were discarded to ensure that sample air was not a mixture of air collected from separate level heights.

The VOCs with related mass-to-charge ratios (m/z) selected for measurement using the PTR-MS technique during these field measurements were methanol (m/z 33+), hexanol fragment (m/z 41+), acetaldehyde (m/z 45+), acetone (m/z 59+), isoprene (m/z 69+), the monoterpenes (primary mass fragment m/z 81+ and m/z 137+) and the parent sesquiterpene ion (m/z 205+). To monitor instrument noise, m/z 25+ (i.e., empty background) was also measured. During the 2016 measurements, the list of VOCs selected for detection by the PTR -MS was extended to include acetic acid (m/z 61+), MVK+MACR (m/z 71+), MEK (m/z 73+), toluene (m/z 93+), terpene fragment (m/z 95+), and the primary sesquiterpene fragment (m/z 149+). A list of mass-to-charge ratios for which the PTR-MS scanned can be seen in Table 1. The calibration of the PTR-MS was checked using a gravimetrically prepared calibration standard (Ionimed Analytik, Innsbruck, Austria). Instrumental sensitivities for methanol, acetonitrile, acetaldehyde, ethanol, acrolein, acetone, isoprene, crotonaldehyde, 2-butanone, benzene, toluene, o-xylene, chlorobenzene, α-pinene, 1,2-dichlorobenzene, and 1,2,4-trichlorobenzene were determined by multi-point calibration. Additionally, using PTR-MS measurements of the m/z 21+ and 37+ ions (Holst et al., 2010), a comparison was performed between the water vapor readings from PTR-MS observations to station reported water vapor to check the long-term stability of the PTR-MS system's performance.

Table 1: A list of the m/z ratios scanned for by the PTR-MS instrument during the full 2014-2016 field campaign measurements at ICOS Norunda. Compound identification for scanned ions is also provided. Abbreviated compounds are MVK (Methyl-vinyl-ketone), MACR (Methacrolein), and MEK (methyl-ethyl-ketone). Dwell times (s) of the PTR-MS scanning sequences and detection limit (pptv) of the measurements are shown for ~~the~~ both 2014-2015 and 2016 campaign periods. Total PTR-MS scanning cycle duration for the 2014-2015 and 2016 campaign periods were ca. 20 and 24 s, respectively. The detection limit (DL) is the signal-to-noise ratio as determined from 2x standard deviation of zero-air background measurements (cps) and the sensitivity (cps pptv[-1]) determined from the campaign-period measurements. Table bottom shows detection limits for the quantified total monoterpene (based on 81+ and 137+ ions) and total sesquiterpene (based on 149+ and 205+) concentrations (pptv).

m/z ratio	dwell times [s]		compound identification	DL [pptv] ($2 \times \sigma_{blank}$/sensitivity)	
	2014-15	2016		2014-15	2016
33+	2.0	1.0	methanol (CH_4O)	274	294
41+	2.0	1.0	hexanol secondary fragment	20.2	32.3
45+	2.0	1.0	acetaldehyde (C_2H_4O)	70.3	90
59+	2.0	1.0	acetone (C_3H_6O)	16.2	62
61+	—	1.0	acetic acid ($C_2H_4O_2$)	—	32
69+	2.0	1.0	isoprene (C_5H_8), methylbutenol fragment	9.74	12.9
71+	—	1.0	MVK, MACR (C_4H_8O)	—	10.2
73+	—	1.0	MEK ($C_4H_{12}O$)	—	18.8
81+	2.0	2.0	monoterpene primary fragment	4.96	6.04
93+	—	2.0	toluene (C_7H_8)	—	10.8
95+	—	2.0	terpene secondary fragment	—	7.38
137+	2.0	2.0	monoterpenes ($C_{10}H_{16}$)	3.32	3.69
149+	—	2.0	sesquiterpene primary fragment	—	3.85
205+	5.0	5.0	sesquiterpenes ($C_{15}H_{24}$)	1.89	1.72
			total monoterpenes (using 81+, 137+)	6.15	7.76
			total sesquiterpenes (using 149+, 205+)	—	6.13

During the 2014-2016 campaign, the PTR- MS was operated with several different measurement sequences as it scanned for different sets of BVOC components. In 2014 and 2015, typical dwell times were 2.0 s, and a typical scanning sequence took

175 about 20 s. In 2016, dwell times were typically either 1 or 2 s, and a scanning sequence took about 24 s. For all years, the
dwell times for the m/z 21+, 25+, 37+, and 205+ ion readings were 0.1, 0.5, 0.1, and 5 s, respectively.

Based on the standard deviation (2σ) of the zero-air background readings of the m/z 21+, 37+, and target ions, the detection
limit of the PTR-MS for the VOC concentration measurements (Table 1), and thus the signal-to-noise ratios (s/n), were
180 calculated. For methanol the mean s/n was relatively high (15.4), and the mean s/n for acetone and acetaldehyde was 7.8 and
3.7, respectively. The lowest mean s/n for non-sesquiterpenes was found for isoprene (1.37) at the 95%-confidence level for
May to end of June 2016. The mean s/n ratio for m/z 81+ and 137+ was 9.8 and 7.1, while the mean s/n ratio for total
monoterpenes (determined from the 137+ and mass-fragment 81+ readings) was somewhat higher (12.8). The majority (>
90%) of 205+ measurements for all campaign years fell below the detection limit.

185

Fragmentation of larger BVOC compounds (> m/z 80+) in the PTR-MS is an important consideration (e.g., Steinbacher et
al., 2004). Monoterpene concentration is determined from m/z 137+ and its primary fragment m/z 81+ (Steinbacher et al.,
2004; Tani et al., 2003). For the 2016 data, an evaluation of total sesquiterpene concentration was conducted from the
concentration of its complete protonated ion (m/z+ 205) and its primary fragment ion (m/z 149+). The vast majority of these
190 total sesquiterpene measurements, however, also failed to exceed the calculated detection limit (6.13 pptv). Given that
sesquiterpene emissions are ubiquitous at boreal forests during summer, such as at Norunda (e.g., Wang et al., 2017), this
indicates that sampled sesquiterpenes were mostly lost to reactions or inlet tubing before the air samples reached the PTR-
MS detector.

2.4 Inversion calculations

195 To quantify the strength of various compound sources and sinks within the forest canopy, Lagrangian dispersion theory was
applied.
Unlike previous investigations which relied on empirical (Raupach et al., 1986) or fitted turbulence profiles (Karl et al.,
2004) for estimating the standard deviation of the vertical wind speed (σ_w), friction velocity (u_*), and Lagrangian time-
scale (T_L), in this analysis we used sonic anemometer measurements from twelve heights to determine the profiles of σ_w,
200 u_*, and T_L. Sonic anemometer data from these heights was processed according to the methodology presented by Mölder
et al. (2004). As Lagrangian timescales T_L cannot be directly measured from one-point measurements (i.e., a sonic
anemometer affixed to a stationary tower), T_L values were calculated from measured Eulerian timescale values T_E based on
the approach of Raupach (1989), using the relationship

205 $$T_L = \beta \frac{\bar{u}}{\sigma_w} T_E ,$$ (1)

where $\bar{u}$ is the mean wind velocity and β is a scaling constant chosen to be equal to one (Raupach et al., 1986). The timescales T_E were defined as the time delay for the autocorrelation function of vertical velocity w to decay to 36.8 % (1/e) of the maximum value (Mölder et al., 2004; Raupach, 1989). The choice of β = 1 at and below canopy height has previously been shown to be a reasonable approximation (Mölder et al., 2004; Raupach, 1989). Twelve source layers were used (from 2m (ca. z/h=0.07) to 100.5m (ca. z/h=3.6)) for the calculation of the source distribution. The six measurement heights for BVOC and ozone were used for interpolation of the concentration gradients at 6.25m, 11.0m, 16.25m, 21.75m, and 29.0 m (ca. z/h = 0.22, 0.39, 0.58, 0.78, and 1.04). The values of σ_w and T_L at 2m were described using the parameterization given by Nemitz et al. (2000). Ground-level BVOC emissions are not separated from emissions in this lowest source layer (thickness 2m) due to the limitations of parameterizing σ_w/u_*/u* near the surface (Wilson and Flesch, 1993).

The ozone and BVOC source/sink distributions in and below the canopy were derived using a Lagrangian dispersion theory approach (Karl et al., 2004; Warland and Thurtell, 2000). In this approach, the source and sink layers in the forest canopy are quantified using dispersion matrix inversion. The dispersion matrix used for analyzing this these data utilized the gradient approach formulated by Warland and Thurtell (2000). The dispersion relation is of the form given by:

$$\frac{dc}{dz}\Big|_i = \sum_{j=1}^m D_{ij} S_j, \tag{2}$$

where the concentration gradient at height z_i is the sum of all contributions from source/sink layers S_j at heights z_i. The elements D_{ij} of the dispersion matrix **D** are calculated as the sum of near-field and far-field dispersion terms (, and are given by Eq A1 in the appendix). For the BVOC compounds investigated by this analysis, chemical processes such as breakdown or creation of compounds directly in atmosphere typically occur on timescales much longer than the canopy mixing timescales used for the Lagrangian dispersion analysis or friction velocity based mixing timescales, leading to quite low Damköhler number (Rinne et al., 2012). Therefore photochemical losses/production are not explicitly parameterized in the inversion analysis procedure and are convoluted with direct sources and sinks.

It is frequently noted that, for Lagrangian dispersion-derived inversions used to calculate source/sink layer strengths, the number of observations should well exceed ($\geq$ x2) the number of prescribed source/sink layers (e.g., Raupach et al., 1986). This is to improve the robustness of the inversion results. Without this condition, instability is a frequent shortcoming of localized near field (LNF) and continuous near field (CNF) models, as noted in Raupach et al. (1986) and Siqueira et al. (2000). To quantify the vertical concentration gradient in the forest canopy using the concentration measurements at the six inlet heights, we fitted a curve to the concentration data (see Figure 3), and the concentration gradient at heights throughout the canopy was quantified from the slope of the fitted curve. For daytime data, a curve was fitted to the concentration data

using a loess fit (Cleveland et al., 1992). The span setting for this loess fit was 0.7. For nighttime data, ~~because~~ as

240   concentration gradients tend to be relatively large due to the often stable nighttime atmosphere (see Figure 3), a concentration curve was established by interpolating between the concentration observations. Figure 3 shows an example of fitted concentration curves for daytime and nighttime monoterpene and CO_2 observations.
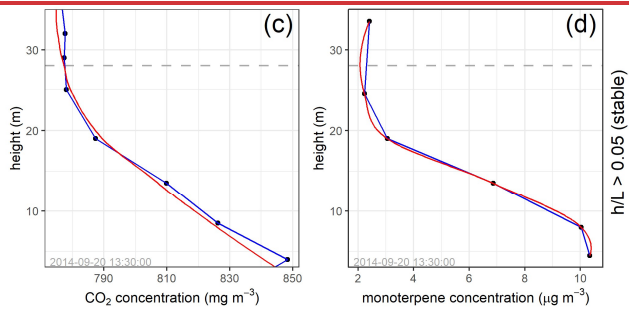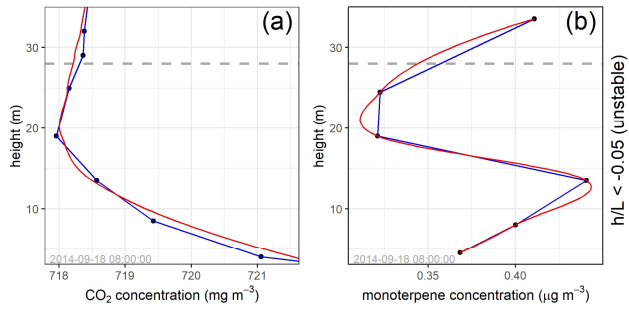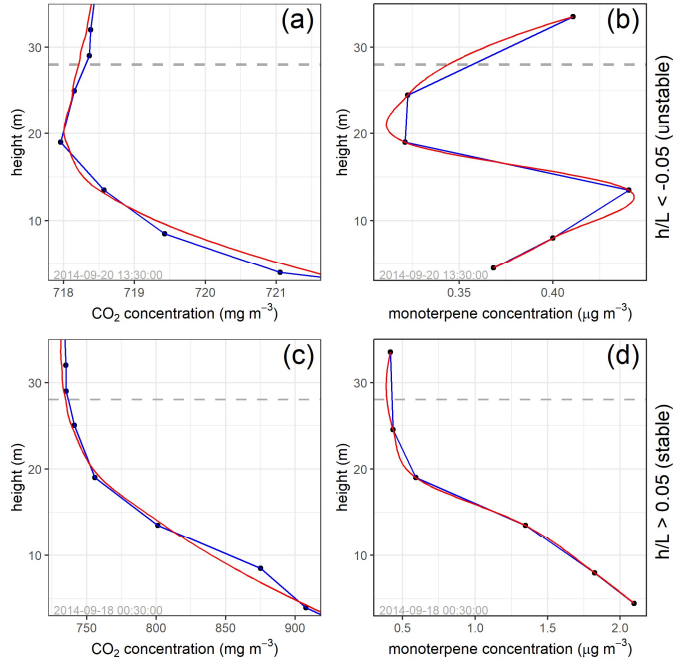
Figure 3: Fitted concentration curves. (a) and (c) show fitted CO$_2$ profiles. (b) and (d) show fitted monoterpene profiles. (a) and (b) show cases with an unstable, daytime atmosphere, while (c) and (d) show cases with stable, nighttime atmospheric conditions. Horizontal dashed line indicates canopy height (28 m).

A damped least-squares approach, weighted by solution smoothness (Siqueira et al., 2000)(Eq. 32), was then applied when performing the inversion, with

$$\boldsymbol{S}^{est} = [\mathbf{D}^{\mathbf{T}}\mathbf{D} + \epsilon^2 \mathbf{W_m}]^{-1} \mathbf{D}^{\mathbf{T}} \left(\frac{dc}{dz}\right), \tag{3}$$

where $\boldsymbol{S}^{est}$ is the vector of estimated source layer strengths, $\mathbf{D}^{\mathbf{T}}$ is the matrix transpose of $\mathbf{D}$, ϵ is a weighting parameter, $\mathbf{W_m}$ is a weighting matrix, and $\boldsymbol{dc/dz}$ is the vector of vertical gradients of the concentration profile at heights z_i.

The use of this weighted minimization procedure (Menke, 2018) comes from the approach suggested by Siqueira et al. (2000), so that the sensitivity of the inversion to variations in the input measurements is addressed by weighted minimization of both least-squares prediction error and a smoothness measure of the source layer strengths S_j, as imposed in Eq. 2 by a weighting matrix $\mathbf{W_m}$. The weighting matrix $\mathbf{W_m}$ is given by Eq. ~~4~~3,

$$
\mathbf{W_m} = \begin{bmatrix} -1 & 1 & 0 & \cdots & \cdots & 0 \\ 0 & -1 & 1 & 0 & \cdots & 0 \\ \vdots & & \ddots & \ddots & & \vdots \\ 0 & \cdots & 0 & -1 & 1 & 0 \\ 0 & \cdots & \cdots & 0 & -1 & 1 \end{bmatrix}^{T} \begin{bmatrix} -1 & 1 & 0 & \cdots & \cdots & 0 \\ 0 & -1 & 1 & 0 & \cdots & 0 \\ \vdots & & \ddots & \ddots & & \vdots \\ 0 & \cdots & 0 & -1 & 1 & 0 \\ 0 & \cdots & \cdots & 0 & -1 & 1 \end{bmatrix}. \tag{4}
$$

The choice of the inversion weighting parameter ϵ for the BVOC and ozone inversions was informed by iterating the inversion calculation over a sequence of ϵ values to quantify the CO_2 source/sink layer strengths in the Norunda canopy, and comparing the modeled CO_2 flux (i.e. sum of the CO_2 source/sink layer strengths in the canopy) to the above-canopy CO_2 flux determined by eddy-covariance (~~measured~~ at 35 m on the flux tower).
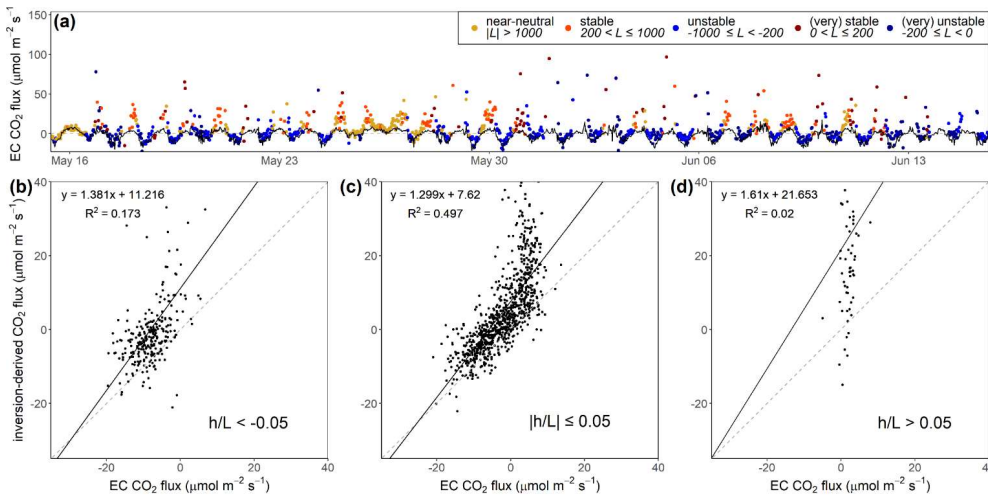
Figure 4: Time series (a) and scatterplots (b-d) showing inferred CO_2 flux from inversions and EC flux measurements. (a) Time series showing measured EC CO_2 flux (black line) and inversion-derived estimate of CO_2 flux (points). Above-canopy stability conditions at 36 m during flux observations - unstable (blue), near-neutral (yellow), and stable (red) - are indicated. Horizontal dashed grey line indicates zero net flux level. Scatterplots show data points sorted by stability parameter h/L for above-canopy stability conditions at 36 m (b) (h/L < -0.05), (c) (|h/L| ≤ 0.05), and (d) (h/L > 0.05). Linear best-fit (black) and R^2 value for panels b-d are shown as well.

CO_2 mixing ratio observations were made at heights from 0.8 m to 101.8 m a.g.l. on the Norunda flux tower. Since BVOC measurements were only collected until slightly above the forest canopy (z/H=1.2, up to 33.5 m), only CO_2 gradient fits from 0.8 m up to 33 m on the tower were used for the inversion calculations. Figure 4 shows the results for these CO_2 inversion calculations. It shows that the best CO_2 inversion-derived flux results are typically achieved during near-neutral atmospheric conditions in the canopy, and that during stable conditions (predominantly observed at night) the inversions tend to overestimate the magnitude of source/sink layer strengths, particularly for positive fluxes out of the forest canopy. Based on the results from comparing inversion-derived to EC-measured CO_2 fluxes, the value of the weighting parameter ϵ for the BVOC and ozone inversions was chosen to be 0.15, based on maximizing the R^2 value (0.76) of the linear best-fit (see Figure 4). It should be noted that inversion model performance is in general impeded in cases of non-stationarity of atmospheric conditions in the canopy and above, such as during the morning transition from a stable surface layer to the development of the convective boundary layer (e.g., Ouwersloot et al., 2012; Siqueira et al., 2003; Vilà-Guerau De Arellano et al., 2009), when the stationarity assumptions inherent in the formulation of the inversion approach are suspect. For example, when CO_2 that has built up in the canopy during stable nighttime conditions, i.e. storage, flushes out during the breakup of the stable boundary layer.

3 Results

A range of reactive VOCs and ozone in the ambient air were detected throughout the Norunda canopy. An overview of the daily median values of daily BVOC and ozone concentrations in the forest canopy (35 m), as well as station meteorological measurements, during the 2014-2016 field campaign periods can be found in Figure 5. The 5th-to-95th percentile range of daily BVOC and ozone concentrations at 35m is shown in Figure 5 as well. Vertical profiles of turbulence statistics from the sonic anemometer measurements for several seasonal time periods (fall 2014, summer 2015, fall 2015, and spring 2016) are shown in Figure 6.

300
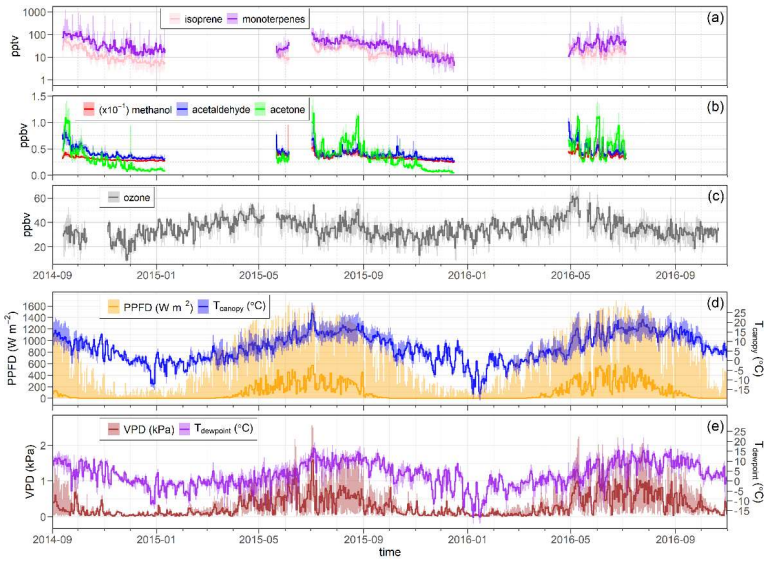
Figure 5: Daily median of the 30-min BVOC concentration (pptv) and ozone concentration (ppbv) sampled at the 33.5 m inlet, as well as related meteorological measurements. Shaded area depicts 5th-to-95th percentile range of daily concentration. (a) Monoterpene and Isoprene concentrations (pptv) shown on a log-scale. (b) Methanol (x10-1), acetaldehyde, and acetone concentrations (ppbv). (c) Ozone concentration (ppbv). (d) PPFD (55 m) and canopy surface temperature (measured by infrared thermometry from 55 m). (e) Vapor pressure deficit and dew-point temperature (at 36.5 m). Canopy height is 28 m. Set of

305 **displayed measurements displayed span from September July 2014 to October 2016.**
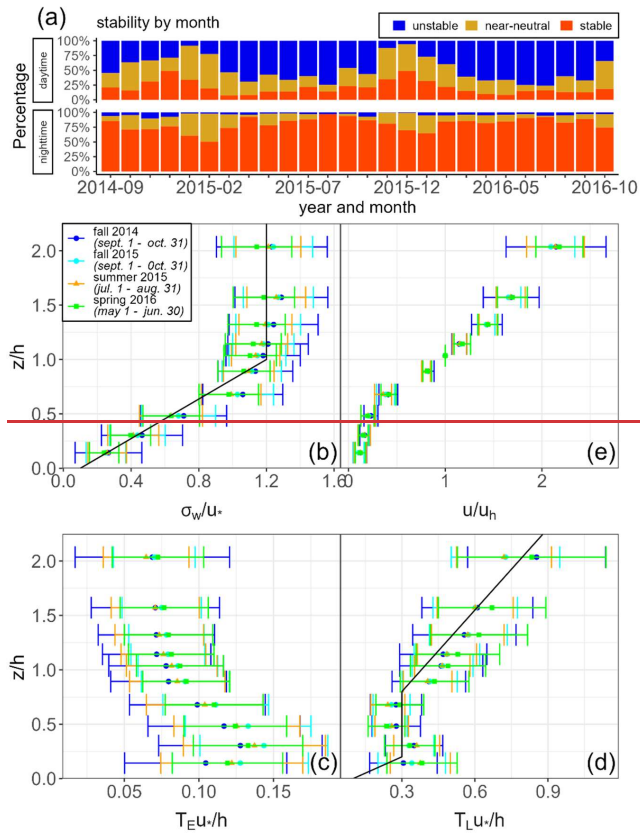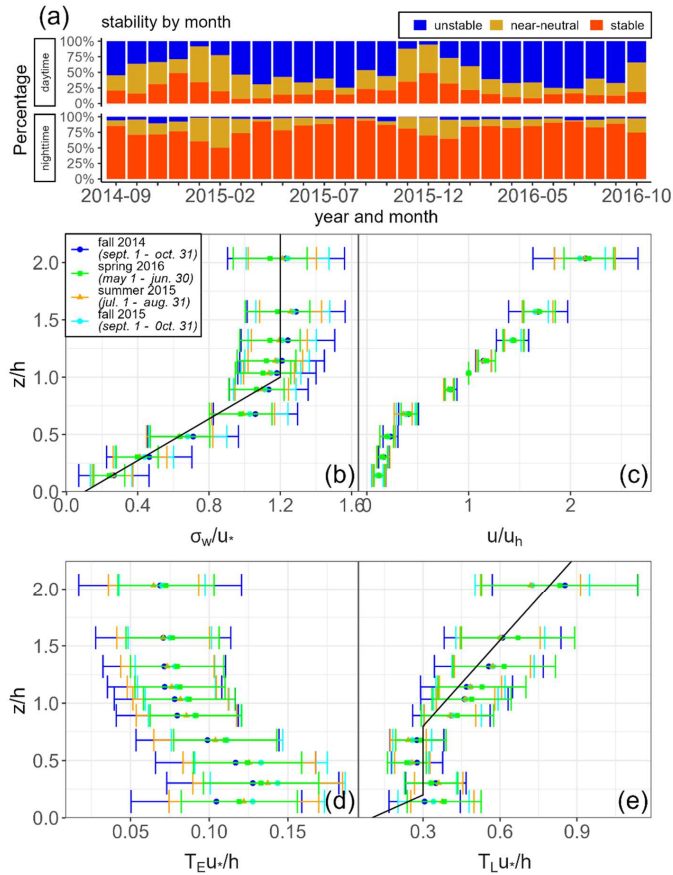
Figure 6: (top) Breakdown of unstable (-1000 < L < 0), near-neutral (|L| > 1000), and stable (0 ≤ L < 1000) conditions in the canopy. (bottom) Vertical profiles for near-neutral conditions of normalized (b) standard deviation of vertical wind velocity σ_w/u_*, (c) ~~mean wind velocity U/U_h (U_h is the velocity at canopy height)~~ Eulerian timescale $T_E u_*/h$, (d) ~~Eulerian timescale $T_E u_*/h$~~ Lagrangian timescale $T_L u_*/h$ and (e) ~~Lagrangian timescale $T_L u_*/h$~~ mean wind velocity U/U_h (U_h is the velocity at canopy height). The black lines, showing empirical fits of normalized σ_w and T_L, are adapted from Mölder et al. (2004). The u_* used to normalize the profiles is measured at top of tower (100.5 m). On the x-axis of these profiles is shown normalized height z/h, where canopy height h is 28 m. Points are determined from 30-minute averaged data, and the standard deviation of these points are plotted as error bars. Data values are shown for fall 2014 & 2015 (dark blue & light blue) for September 1st to October 31st, summer 2015 (orange) for July 1st to August 31st, and spring 2016 (green) for May 1st to June 30th. During the fall 2014 period, there were 664 (23.1 %) unstable, 744 (25.9 %) near-neutral, and 1469 (51.1 %) stable data points. During the summer 2015, there were 1191 (42.2 %) unstable, 311 (11 %) near-neutral, and 1319 (46.8 %) stable data points. During the fall 2015 period, there were 647 (24.4

320 **%) unstable, 375 (14.1 %) near-neutral, and 1633 (61.5 %) stable data points. During the spring-2016 period, there were 1393 (48.6 %) unstable, 450 (15.7 %) near-neutral, and 1025 (35.7 %) stable data points.**

3.1 BVOC and ozone observations

During the growing season methanol was detected in the range of 3.0 to 5.1 ppbv throughout the canopy. Peak

325 concentrations in the canopy were typically observed during nighttime under stable atmospheric conditions in the canopy. Isoprene concentrations were observed to be low in the seasonal observations (e.g., approximately 250 pptv maximum concentration during summer 2015). Given previous branch-level measurements (Wang et al., 2017), this indicates that there is no particularly strong source of isoprene in the forest canopy. Daily median ozone concentrations (at 33.5m) for the full measurement campaigns can also be seen in Figure 5. Ozone concentrations typically ranged from 30 to 60 ppbv during the

330 growing season, with peak concentrations typically observed above-canopy during the afternoon and minimum typically observed near forest-floor at or near sunrise (Figure 7).
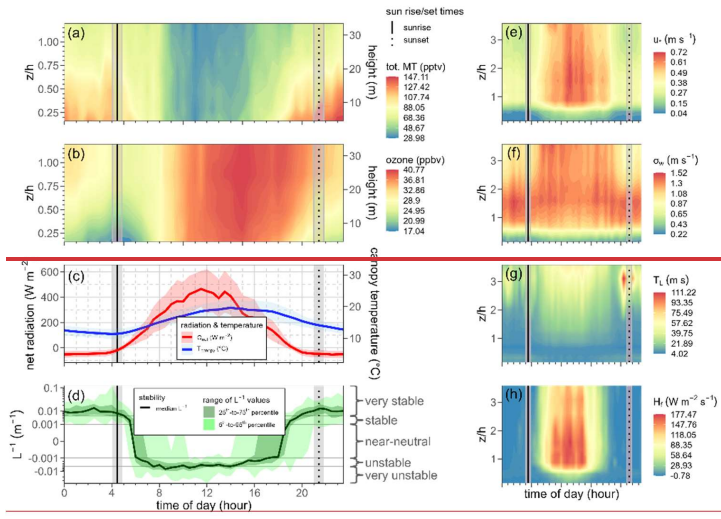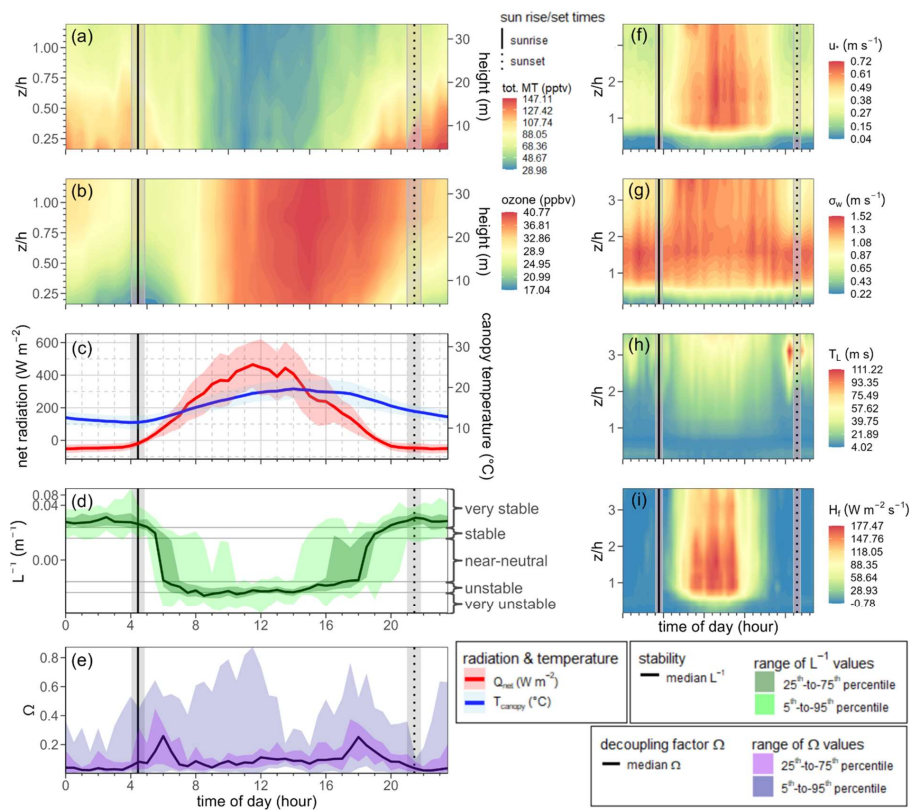
Figure 7: Mean diurnal cycle of (a) monoterpene and (b) ozone profile concentrations for a clear-weather period of summer 2015 (July 20th to August 10th). (c) Net radiation (red) and canopy temperature (blue). Net radiation and canopy temperature are measured from 55 m. Shaded regions of net radiation and canopy temperature indicate one standard deviation. (d) Plot of the inverse of the Obukhov length (L^{-1}), indicating the atmospheric stability above the canopy (measured at 36 m). Classification of stability from Obukhov-length (L) values (very stable: $0 \leq L < 200$, stable: $200 \leq L < 1000$, near-neutral: $1000 \leq |L|$, unstable: $-1000 < L \leq -200$, very unstable: $-200 < L \leq 0$). (e) Plot of the decoupling factor Ω, indicating the degree of aerodynamic coupling between canopy vegetation and the atmosphere above the forest canopy. See Appendix for more details regarding Ω. (fe) Diurnal mean contour profiles of friction velocity u_* (m s^{-1}), (gf) standard deviation in vertical wind velocity σ_w (m s^{-1}), (hg) Lagrangian timescale (s), and (if) sensible heat flux H_f (W m^{-2} s^{-1}) with respect to the normalized height z/h in the forest. In all panels, sunrise (solid vertical line) and sunset (dotted vertical line) are indicated. Shaded region indicates the range of sunrise and sunset times during the July 20th to August 10th period.

3.1.1 Isoprenoids

Typically for a forest with a tree species composition such a Norunda, isoprene concentrations peak in the summer months. Isoprene concentrations were below 20 pptv in the autumn, less than 5% of the time concentrations exceeded 35 pptv, the mean concentration being 20 pptv. The maximum value occurred during daylight hours, at a time when temperature and PPFD were high (>20°C and >1000 W m^{-2}) as well, with concentrations falling to daily lows at all measurement heights towards the evening. The inversion results for isoprene are also consistent with its emission being light-dependent, with the source profiles indicating there being (an albeit weak) canopy source during the day. As expected, little to no isoprene emission was observed at night. The nighttime inversion profile (known to be biased toward overpredicting source strengths due to nighttime conditions (e.g., Siqueira et al., 2002; Siqueira et al., 2000)), show negligible source layer strength for isoprene during nighttime hours from July 15th to August 15th, 2015 (< 0.3 ng m^{-2} s^{-1} / level, with 0.64 ng m^{-2} s^{-1} for total inferred flux out of canopy).

Like isoprene, monoterpene concentrations at Norunda were typically highest in summer months. Peak monoterpene concentrations (1 - 1.4 ppbv) in the canopy were an order of magnitude larger than isoprene concentrations. Monoterpene concentrations near the forest floor peaked during night, while monoterpene concentrations in and above the canopy level typically peaked during or slightly following sunrise. An example showing the morning concentration behavior of monoterpenes is shown in Figure 7. This can be due partly to the delay between sunrise (with increasing temperatures) and the development of a well-mixed boundary layer through the stable nocturnal boundary layer.

3.1.2 Water-soluble BVOCs

The summertime high methanol concentration was typically observed in August, with a median concentration of 4 ppb being observed in August 2015 (see Figure 5). Within the canopy, there was a noticeable decrease in concentrations from mid-May to June. Inversion results (see Section 3.3) indicate that this was likely due to strong sinks in the canopy. The highest methanol concentrations were also typically observed in spring, with a median concentration of 4.4 ppb being observed in mid-April 2016. Median methanol concentrations of 4.1 and 4.2 ppbv were observed in May 2015 and 2016, respectively. Acetaldehyde exhibited a similar high springtime concentration tendency as methanol. Acetone had a minimum concentration in the autumn, and peak concentration in August. From August, acetone concentrations above and within the canopy decreased markedly with the progression of fall, to a greater degree percentage-wise than the other PTR-MS measured compounds.

3.1.3 Other VOCs (2016 observations)

From the 2016 data, toluene concentrations were generally low during daytime (ca. 15 pptv) and increased during nighttime (up to 60 pptv). This is consistent with the build-up of evenly distributed anthropogenic background emissions during night

into the shallow nocturnal boundary layer (Karl et al. 2004). Similarly for m/z 95+, which typically had a daytime low concentration (9 pptv), and maximum during nighttime (ca. 40 pptv).

380

During spring 2016, acetic acid concentrations tend to be at a minimum following sunrise (60 pptv), and gradually increased throughout the day until peaking before sunset (ca. 150 pptv), at which point concentrations typically decreaseds until the next sunrise. The exception to this trend appears to be when there was a persistent high nighttime concentration in the canopy, which was associated with similar peaks in acetone, acetaldehyde, and methanol concentrations in the canopy.

385 Unlike many other compounds, the acetic acid concentrations in the forest canopy were higher in the first two weeks of May than in the last two weeks of June. The diurnal concentration of m/z 41+, associated with the PTR-MS protonation process as a hexanol fragment, typically followed a similar pattern to acetone. Minimum in m/z 41+ concentration (about 50 pptv) typically occured in morning following sunrise. Concentrations then usually peaked after sunset (about 130 pptv).

390 For May to June 2016, the mean MVK+MACR concentration was 12 pptv. For June to July 2016, the mean MVK+MACR concentration increased to 19 pptv. From the 2016 measurements, we can estimate the photochemical loss from the ratio of isoprene to MVK+MACR, if we assume turbulent exchange times of approximately 50 - 110 s during daytime, with this timescale based on the far-field limit of Lagrangian dispersion, $\sigma_z = \sqrt{2\sigma_w T_L (t - T_L)}$ (e.g., Raupach, 1989). For this summer period, following the approach of Karl et al. (2004) it was estimated that less than 10% of isoprene was oxidized

395 within canopy. Figure 8 shows the isoprene to MVK-MACR ratios for the 2016 measurements. The range of observed MEK concentrations was 30 – 150 pptv, and was comparable to those reported by Ruuskanen et al. (2009) for a similar boreal forest site.
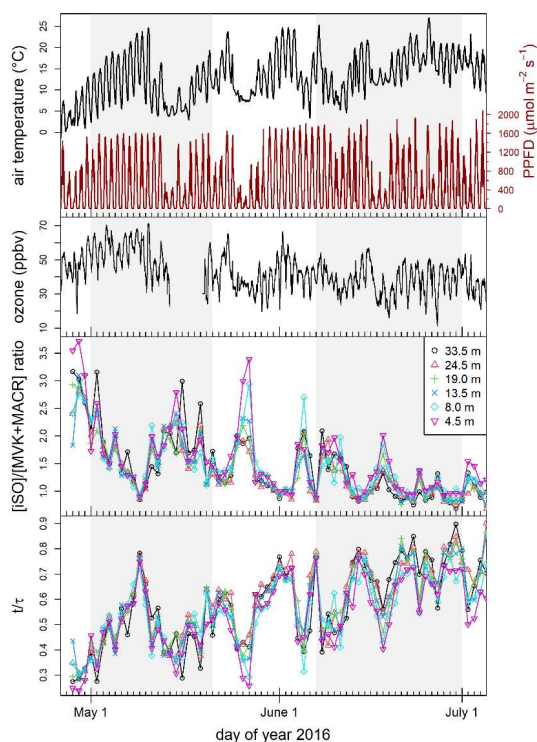
|400 **Figure 8: Daytime ratio of isoprene to MVK+MACR ~~during~~ from May 1 to July 1, 2016. (top panel) air temperature (°C) (black), PPFD (µmol m⁻² s⁻¹) (red), and ozone (ppbv) (black), (middle panel) the ratio of isoprene to the oxidation products MVK & MACR, and (bottom panel) the ratio of time t progressed to time-constant τ vs day of year. Air temperature and PPFD displayed ~~are~~ were measured at 35 m and ozone ~~measured~~ at 33.5 m. The two shaded areas indicate the two seasonal time periods presented in Figure 10.**

405

3.2 Source/sink inversion results

The seasonal average source and sink distributions for isoprene, monoterpenes, methanol, acetaldehyde, and acetone, are plotted in Figure 9. For summer 2015, the average inversion-derived isoprene daytime flux for the four-week period shown in Figure 9 was 7.3 µg m⁻² h⁻¹. The highest emissions of monoterpene occur~~ed~~s during summer in the upper part of the

410 canopy (at approx. 25 m). The average inversion-derived daytime monoterpene flux for ~~that~~ this four-week period was 120 µg m⁻² h⁻¹ (± 30.3 µg m⁻² h⁻¹), with a source strength up to 9.7 ng m⁻² s⁻¹ /level (±34.6 µg m⁻² h⁻¹ /level) found in the mid-

canopy (i.e., layer from 19 to 25 m). These values are consistent with strong MT emissions previously reported at ICOS Norunda during this seasonal time period (Wang et al. 2017).
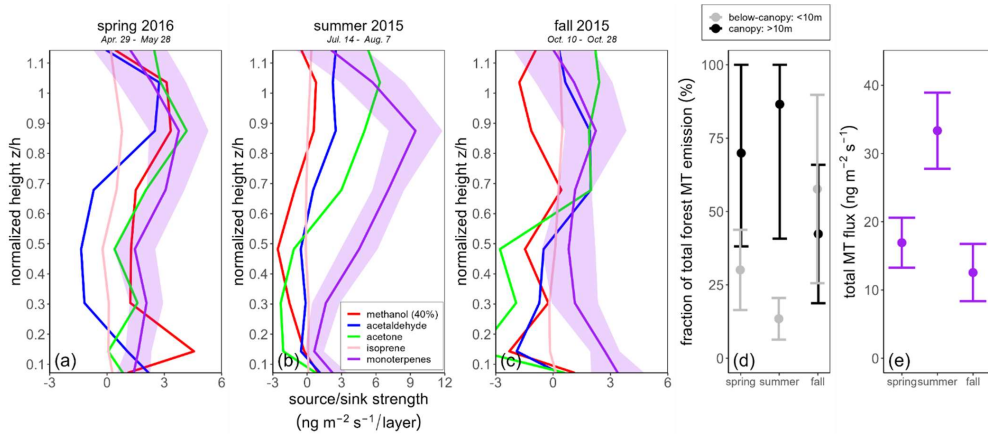
415

Figure 9: Seasonal ~~BVOC~~PTR-MS inversion results for the canopy source and sink profile distribution. (a-c) Data shown represent the average of daytime concentrations (for 1.5 hours after sunrise to 1.5 hours before sunset) for (a) summer 2015, July 14th to August 7th, (b) fall 2015, October 1st to October 28th, and (c) spring 2016, April 29th to May 28th. Shaded region for monoterpenes indicates ± standard error. (d) Relative contribution to total monoterpene emission from the canopy (black) and
420 **from below-canopy (gray), and (e) total inferred monoterpene flux (purple), for spring 2016, summer 2015, and fall 2015 periods shown in (a-c).**

The relative seasonal contribution from canopy and below-canopy to total forest MT emissions in spring, summer, and fall was quantified from the daytime source profiles presented in Figure 9. The uncertainty range for the % relative contribution
425 to total inferred MT flux from canopy and below-canopy was quantified by standard error propagation. During summer 2015, for the total-inversion derived daytime MT flux of 120 μg m^{-2} h^{-1}, an average of 86.4% originated from the canopy and 13.6% from below-canopy. During fall 2015, for an inferred daytime MT flux of 45.2 μg m^{-2} h^{-1} (± 17.6 μg m^{-2} h^{-1}), an average of 42.3% came from the canopy and 57.7% from below-canopy. During spring 2016, for a total-inversion derived daytime MT flux of 60.9 μg m^{-2} h^{-1} (± 18.44 μg m^{-2} h^{-1}), an average of 69.9% came from canopy and 30.1% from below-
430 canopy.

The 2016 ~~PTR-MS~~ BVOC inversion results for two spring and early-summer periods (May 1st to May 24th and June 7th to July 1st, respectively) for the canopy source and sink profile distributions are shown in Figure 10, showing how the inversion-derived distribution of sources and sinks evolves from the spring to summer growing seasons for the expanded list
435 of VOC compounds that were monitored during this period. For this 2016 period, the typical daytime inversion-derived

ozone flux was found to vary between approximately -0.3 and -0.9 μg m^{-2} s^{-1}. From this ozone flux, we derive an ozone deposition velocity that varies between approximately 0.4 and 0.9 cm s^{-1}.
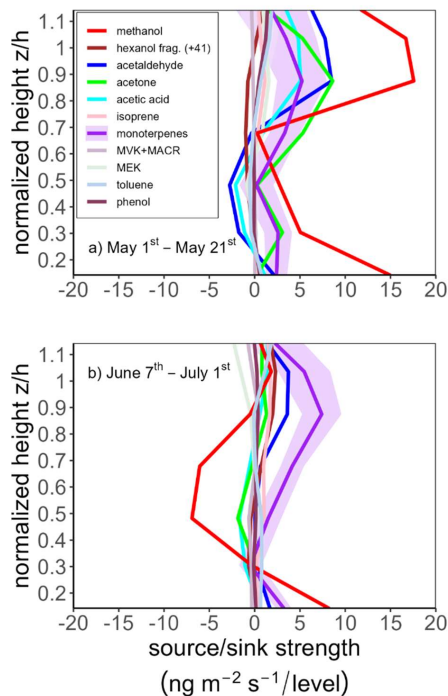
440 **Figure 10: 2016 ~~PTR-MS~~BVOC inversion results for the canopy source and sink profile distribution. Data shown represent the average of daytime concentrations (for 1.5 hr after sunrise to 1.5 hr before sunset) from (top panel) May 1st to May 21st and (bottom panel) June 7th to July 1st, 2016. Shaded region for monoterpenes indicates ± standard error. The flux tower air temperature and PAR during these time periods are shown in the top panel of Figure 8.**

445 While daytime concentrations for methanol, acetaldehyde, and acetone often followed a predictable behavior for a particular season, it was observed that the relative nighttime concentration patterns could be quite variable, particularly at a seasonal scale between autumn, and spring and summer seasons. An example of this variability is presented in Figure 11. Strong enhancement of nighttime sinks of water-soluble BVOC compounds (i.e., methanol, acetaldehyde, and acetone) is noted to frequently coincide with the presence of favorable dew-forming conditions in the forest canopy.

450
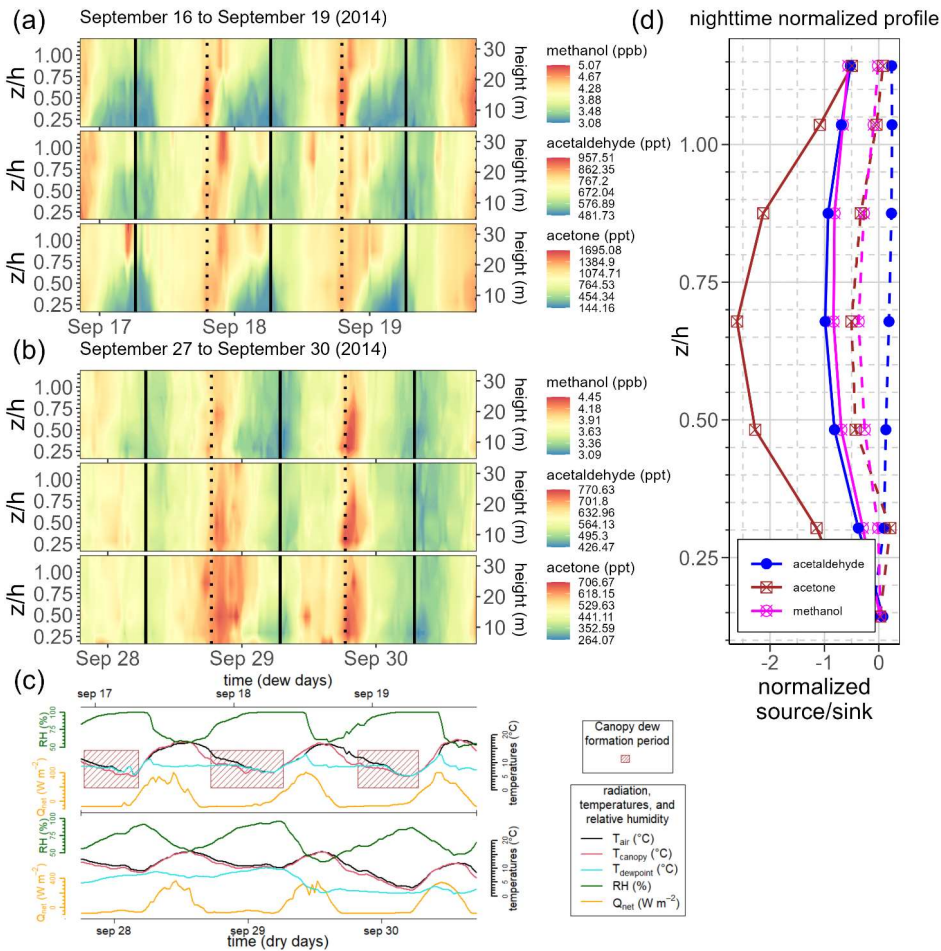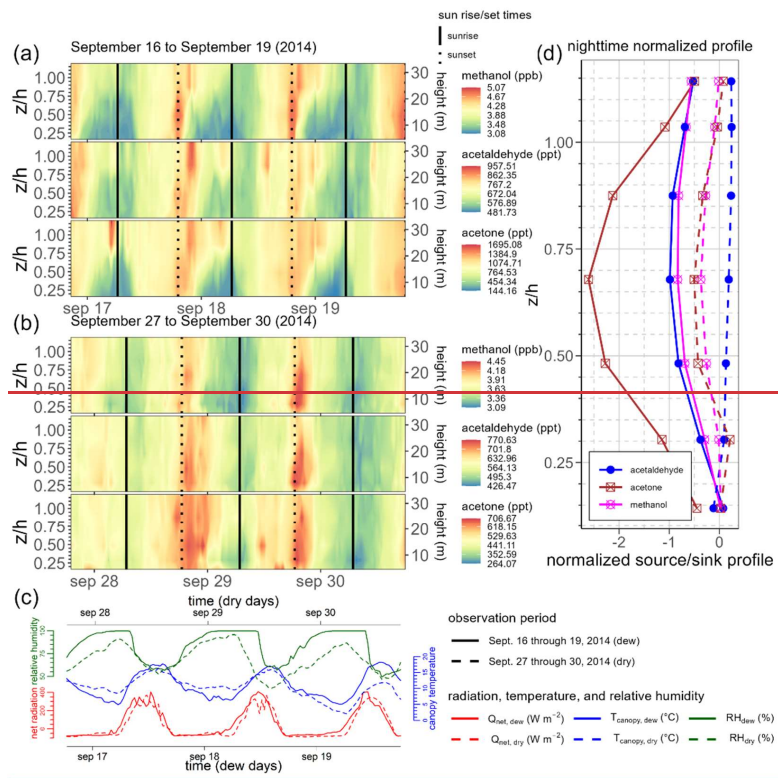
Figure 11: Nighttime dew effects on water-soluble BVOCs in forest canopy. (a) Methanol concentration profile from Sept. 16th to 19th, during conditions where nighttime dew is assumed to have formed in the forest canopy. (b) Methanol concentration profile two weeks later, from Sept. 27th to 30th, during dry conditions. In a) and b), sunrise (solid vertical line) and sunset (dotted vertical line) are indicated. (c) 3-day time-series for meteorological conditions during the "dry" period from the 16th to 19th (~~dashed~~bottom-of-panel) and during "dew" periods (~~solid line~~top-of-panel). The meteorological values shown are air temperature (black) in the canopy (at 28 m), IR-measured canopy surface temperature (red), dewpoint temperature (cyan) in the canopy (at 28 m), relative humidity (green), and net radiation (~~orange~~red).~~, canopy temperature (blue), and relative humidity (black). RR~~Relative humidity is measured at 28~~36~~ m. Time periods when dew is expected to have formed in the forest canopy during the "dew" periods are indicated in panel (c) with brown boxes. (d) Normalized source and sink profiles, for methanol, acetaldehyde, and acetone, during the dew and dry periods. Both left- and right-panel profiles are normalized by the sum of the dry period profile level strengths.

4 Discussion

The isoprene inversion results show a clear diurnal behavior for isoprene emission. The range of observed isoprene concentrations, while relatively low, is consistent with a spruce and pine boreal forest (e.g., Hakola et al., 2017; Rinne et al., 2005) such as Norunda, as well as with values previously reported at the station (Wang et al., 2017).

A local maximum in MT concentrations is frequently observed to occur just prior, during or just after sunrise (for example, see Figure 7). This can take place due to a combination of factors, primarily the rise in the needle temperature following sunrise, followed later by the morning onset of hydrostatic instability in the canopy. For example, there was~~is~~ frequently a change in canopy turbulence profile occurring around the same time as sunrise, with the profile switching from stable or highly stable to unstable or highly unstable as characterized by the Obukhov length L. This was~~is~~ coincident or immediately following in time with the rise in canopy temperature and net radiation occurring with sunrise. The same phenomena is well known from previous studies of forest CO_2 concentrations (e.g., Aubinet et al., 2012). Diurnal changes in plant needle physiology would not seem to contribute much to this occasional morning burst behavior. Niinemets and Reichstein (2003) rule out stomata as effectively controlling the emission rates of VOC compounds with a Henry's law constant exceeding approximately 100 Pa m^3 mol^{-1}. Given typical values of Henry's law constant for monoterpenes, from approximately 2615 Pa m^3 mol^{-1} for γ-terpinene to 13560 Pa m^3 mol^{-1} for α-pinene (Copolovici and Niinemets, 2005) , this would seem to rule out a stomatal-controlled morning burst in monoterpene emissions.

Scaling up the seasonal inversion results, for the 2015 to 2016 measurements (May through October), the average daytime flux per kilometer of forest during the growing season for isoprene and monoterpenes is estimated to be approximately 205 and 1803 g km^{-1} day^{-1} (ca. 9 and 75 µg m^{-2} h^{-1}). Within a few percentage points, these values are consistent with the summer terpene mass fractions (6% isoprene and 65 % monoterpenes) previously reported at Norunda by Wang et al. (2017).

The monoterpene emission from canopy relative to below-canopy increased (with ca. 70% to 86% from canopy) from spring to summer. In autumn, meanwhile, emissions from canopy and below-canopy ~~are~~ were of similar magnitude (ca. 42% vs. 58%, respectively). Past studies have shown that needle litter in boreal forests can be a prominent contributor to BVOC emissions in autumn, particularly for monoterpenes (Aaltonen et al., 2011; Kainulainen and Holopainen, 2002). The same is true for enhanced autumn emissions of monoterpenes observed in boreal forests due to soil microbial activity (Mäki et al., 2019b). It is possible that litter deposited the previous year may also have contributed in part to the relatively closer fraction in springtime (ca. 30% vs 70%, compared to 14% vs 86% in summer 2015) found earlier in the growing season, as a large portion of the forest needle litter ~~does~~ may not have decomposed nor released from needle storage as efficiently, due to decreasing temperatures in autumn and winter, until the following spring (e.g., Aaltonen et al., 2011; Wang et al., 2018).

Of all the BVOC compounds observed, methanol has perhaps the most variable distribution of sources and sinks in the canopy at a seasonal timescale. The methanol source profiles derived by the Lagrangian inversions featured strong increases in canopy methanol sources during late April to early May, corresponding in time with new spring growth and conifer budding at the start of the growing season. Methanol production is strongly associated with plant tissue growth (such as during spring and nighttime growth), particularly pectin demethylation in cell wall formation processes (Galbally and Kirstine, 2002; Hüve et al., 2007; Macdonald and Fall, 1993b).

In both 2015 and 2016, while there were no substantial methanol sources inferred from the Lagrangian inversions just below the main bulk of the canopy (25m) during this seasonal period, there was also a large source (lowest source layer at 4 m) near the forest floor. For the spring growing season, if the 4m-layer source is taken as indicative of fluxes from the forest floor, then the inversion-inferred springtime methanol emissions from and just above the forest floor at Norunda are on par with the weekly mean surface methanol emissions observed at other boreal forest sites (Mäki et al., 2019a). Likewise, as observed by long-term surface chamber measurements in Mäki et al. (2019a), the bulk of forest floor VOC exchange inferred from the Lagrangian inversion model appears to be predominantly monoterpenes and methanol.

Meanwhile, another frequent feature that was present in the Lagrangian inversion results was the episodic enhancement of nighttime sinks in the canopy of methanol, as well as acetone and acetaldehyde. It is well known that dew can play a role in the deposition of reactive trace gases to wet surfaces (e.g., Chameides, 1987; Karl et al., 2004; Zhou et al., 2017; Wohlfahrt et al., 2015). For the 2014 – 2016 campaign measurements of methanol and other compounds like acetone and acetaldehyde, it was clear in the inversion results that, for the majority of nighttime periods in summer and fall when the conditions for dew to form on canopy surfaces was were present, a strong enhancement of sink behavior manifested in the forest canopy as well. The fact thatat these sink enhancements occur in the nighttime inversion observations for water-soluble BVOCs, but did not for compounds with a large Henry's law constant like isoprene and the monoterpenes, further supports that this is a dew-deposition related effect. Acetone and acetaldehyde featured similar nighttime sink behavior to methanol in the Lagrangian inversion results when dew was present on canopy surfaces, but not to the same magnitude as methanol. This observation is consistent with the Henry's law constant values of methanol, acetone, and acetaldehyde, as the value is an order of magnitude lower for methanol than the other two compounds (e.g., Niinemets and Reichstein, 2003).

Even though daytime net flux of acetone and acetaldehyde tend to be quite similar, the observed pattern of source and sink layers in the forest canopy, i.e. the distribution of layers, tended to be very different. In terms of the observed pattern of source and sink layers in the forest canopy, though daytime net flux of acetone and acetaldehyde tend to be quite similar, the distribution of layers tends to be very different. Our spring and summer source profiles indicated that the distribution of acetone sources tapereds more sharply approaching canopy top than acetaldehyde, which tends to have had a strong sources

530   high to middle-way up the canopy (top three source layers), followed by a weak sink below the main canopy (13.5 and 8.5 m layers), and a source near the surface (4 m layer).

Previous studies have also considered the canopy distribution of acetone and acetaldehyde sources. For example, with cuvette measurements, Cojocariu et al. (2004) observed smoothly declining acetaldehyde emissions from the top to the
535   bottom of a spruce forest canopy, while for a tropical forest Karl et al. (2004) found for a tropical forest a strong source maximum at the very top of the canopy crown, a sink in the lower part of the crown, and a source region corresponding to the understory.

Two known pathways for acetaldehyde emission are the conversion of cytosolic pyruvate and the oxidation of ethanol
540   (Cojocariu et al., 2004; Kreuzwieser et al., 1999). The cytosolic pyruvate path is associated with the accumulation of pyruvate in the plant cell cytosol and subsequent burst in pyruvate decarbonxylase reactions (Karl et al., 2002), consistently observed in laboratory studies during light-dark transitions (e.g., Kreuzwieser et al., 2000). The ethanol oxidation path can cause acetaldehyde emission in leaves (e.g., Kreuzwieser et al., 2000; Kreuzwieser et al., 1999). The production of ethanol is associated with hypoxic or anoxic conditions occurring in the roots (Kreuzwieser et al., 2000) and transport of ethanol
545   through the xylem to leaves and needles, where it can be released through stomata. Compared to acetaldehyde, relatively less little experimental information is available on the production and emission pathways for acetone. It has been previously hypothesized that acetone is produced in spruce needles by acetoacetate decarboxylation (Macdonald and Fall, 1993a). Afternoon concentration increased in the relatively longer-lived compounds acetaldehyde, acetone, and methanol. These increases occurred from around mid-afternoon to before sunset (see Figure 11), and were most likely due to decreased
550   turbulence and the formation of a stable nocturnal boundary layer (e.g., Karl et al., 2004).

As with the Karl et al. (2004) investigation, albeit in a boreal rather than tropical setting, we attribute our acetaldehyde source distribution to reflect a combination of the two known acetaldehyde emission pathways, with a light-induced increase in overall acetaldehyde emission due to the pyruvate pathway (i.e., alternating light-dark shading conditions) higher up in the
555   forest canopy. Interestingly, in the 2016, campaign data during whichwhen acetic acid was measured, high canopy concentrations of acetic acid early in the day seemeds to presage strong peaks in other compounds monitored in the afternoon and evening. The canopy often appeareds to be a sink of acetic acid from the atmosphere, but during days with increased metabolic activity in the forest canopy (temp > 25 C, PPFD near saturation), the forest also appeareds to be a source of acetic acid, during daytime and often later the following night. It is known that production and use of acetic acid in
560   plants is linked to metabolism and biosynthesis activity via the hydrolysis and reactivation of the intermediate acetyl-CoA (e.g., Liedvogel and Stumpf, 1982). Another source of acetic acid in plants, linked to the production of acetaldehyde, is the pyruvate dehydrogenase pathway, whereby pyruvate is decarboxylated to acetaldehyde, which is then oxidized to acetic acid (e.g., Jardine et al., 2010). During daytime, overall the forest appears to be in general a net sink of acetic acid (see Figure

10). It would be of interest in future studies to investigate the emission of acetic acid from the Norunda forest or similar boreal forests during the fall season, when other ecosystem processes, such as senescence, might be expected to be taking place.

5 Conclusions

In this study, vertical profiles of BVOC, ozone, and turbulence parameters were measured in a boreal forest canopy during several seasonal periods from 2014 to 2016, providing new insight into BVOC exchange processes in boreal forest. A Lagrangian dispersion methodology was developed to investigate the distribution of BVOC and ozone sources and sinks in the Norunda boreal forest canopy. Our results show complex seasonal behavior in source and sink characteristics for BVOCs within this forest canopy, indicating that further investigations seeking additional insight of BVOC emission and deposition properties within boreal forest ecosystems is warranted.

From the Lagrangian dispersion analysis, the monoterpene source strength was found to typically peak mid-canopy (approx. 25 m), while we observed a strong source near the surface (4 m layer) during the autumn. The monoterpene emission from canopy relative to below-canopy increased (with ca. 70% to 86% from canopy) from spring to summer, while in autumn, emissions from canopy and below-canopy were found to be similar in magnitude. The increased relative emissions from below-canopy are attributed to increased understory litter and soil emissions during the autumn (Wang et al., 2018).

Relatively low levels of isoprene (summer mean approx. 25 pptv) were observed in the canopy. As the forest is predominantly composed of Norway spruce and Scots pine, known to be low/none emitters of isoprene, this is consistent with the composition of the forest and previous isoprenoid measurements at Norunda (Wang et al., 2017).

An enhancement in canopy and understory methanol sources was observed in the Lagrangian inversion results during the spring growing season, and attributed to increased methanol production and emission by new growth. Strong episodic nighttime enhancement of nighttime sinks of methanol and other water-soluble BVOCs was noted in summer and fall periods, and was most likely associated with deposition to wet surfaces due to the formation of nighttime dew in the canopy. Both the concentration profile and the inversion results for ozone indicate that the canopy is a significant daytime ozone sink. This likely produces a vertical canopy gradient for the photochemical lifetimes of short-lived (1-20 s) BVOC compounds, such as sesquiterpenes.

While it is generally evident that eddy-covariance (or often other surface layer flux measurement approaches (e.g., Rantala et al., 2014) for that matter) provides greater quantitative resolution in determining ecosystem fluxes than any inverse Lagrangian dispersion approach, the application of inverse Lagrangian modeling to PTR-MSBVOC canopy profile

measurements nonetheless fulfils a clear and useful role in filling the gap between bottom-up (e.g. branch level emissions) and top-down (e.g. ecosystem scale flux) measurements for BVOC emission studies in boreal forest ecosystems. A specific understanding of gas-phase processes within the forest canopy, and the species-resolved source/sink strength distribution of a forest region (Roldin et al., 2019; Thomsen et al., 2021) is important to assess e.g. the impact of boreal ecosystems on the formation of SOA and their impact on the regional radiative forcing (Paasonen et al., 2013).

Appendix A

Equation A1:

$$D_{ij} = \left\{ \frac{-\left[1 - \exp\left(\frac{-(z_i - z_j)^2}{2\Delta z_j^2}\right)\right]}{2\sigma_w^2(z_i) * T_L(z_i) * \left[1 - exp\left(-\sqrt{\frac{\pi}{2}}\frac{(z_i - z_j)}{\frac{[\sigma_w(z_i) * T_L(z_i) + \sigma_w(z_j) * T_L(z_j)]}{2}}\right)\right]} \right.$$

$$\left. - \frac{\left[1 - \exp\left(\frac{-(z_i + z_j)^2}{2\Delta z_j^2}\right)\right]}{2\sigma_w^2(z_i) * T_L(z_i) * \left[1 - exp\left(-\sqrt{\frac{\pi}{2}}\frac{(z_i + z_j)}{\frac{[\sigma_w(z_i) * T_L(z_i) + \sigma_w(z_j) * T_L(z_j)]}{2}}\right)\right]} \right\}, \quad \text{for } z_i > z_j$$

$$D_{ij} = \left\{ \frac{-\left[1 - \exp\left(\frac{-(z_i + z_j)^2}{2\Delta z_j^2}\right)\right]}{2\sigma_w^2(z_i) * T_L(z_i) * \left[1 - exp\left(-\sqrt{\frac{\pi}{2}}\frac{(z_i + z_j)}{\frac{[\sigma_w(z_i) * T_L(z_i) + \sigma_w(z_j) * T_L(z_j)]}{2}}\right)\right]} \right\}, \quad \text{for } z_i = z_j \text{ and}$$

$$D_{ij} = \left\{ \frac{-\left[1 - \exp\left(\frac{-(z_i - z_j)^2}{2\Delta z_j^2}\right)\right]}{2\sigma_w^2(z_i) * T_L(z_i) * \left[1 - \exp\left(-\sqrt{\frac{\pi}{2}} \frac{(z_j - z_i)}{\frac{[\sigma_w(z_i) * T_L(z_i) + \sigma_w(z_j) * T_L(z_j)]}{2}}\right)\right]} \right.$$

$$\left. - \frac{\left[1 - \exp\left(\frac{-(z_i + z_j)^2}{2\Delta z_j^2}\right)\right]}{2\sigma_w^2(z_i) * T_L(z_i) * \left[1 - \exp\left(-\sqrt{\frac{\pi}{2}} \frac{(z_i + z_j)}{\frac{[\sigma_w(z_i) * T_L(z_i) + \sigma_w(z_j) * T_L(z_j)]}{2}}\right)\right]} \right\}, \quad \text{for } z_i < z_j.$$

(A1)

615

Where z_i are the concentration gradient heights, z_j are the source layer heights, and Δz_j is the thickness of the source layers.

620   Table 1A:

height (m)	Fall 2014 (Sept. 1 – Oct. 31)		Summer 2015 (Jul. 1 – Aug 31)		Fall 2015 (Sept. 1 – Oct. 31)		Spring 2016 (May 1 – Jun. 30)	
	σ_w/u_*	T_L	σ_w/u_*	T_L	σ_w/u_*	T_L	σ_w/u_*	T_L
4	0.27 (0.2)	0.31 (0.14)	0.26 (0.11)	0.38 (0.12)	0.25 (0.12)	0.34 (0.14)	0.24 (0.09)	0.38 (0.14)
8.5	0.46 (0.24)	0.35 (0.12)	0.41 (0.15)	0.36 (0.09)	0.44 (0.16)	0.33 (0.1)	0.4 (0.12)	0.33 (0.1)
13.5	0.71 (0.25)	0.28 (0.1)	0.64 (0.19)	0.26 (0.07)	0.68 (0.22)	0.25 (0.07)	0.64 (0.17)	0.24 (0.08)
19	1.06 (0.24)	0.28 (0.11)	0.99 (0.18)	0.24 (0.07)	1.03 (0.21)	0.26 (0.08)	0.98 (0.18)	0.29 (0.1)
25	1.13 (0.22)	0.41 (0.15)	1.1 (0.15)	0.41 (0.1)	1.11 (0.18)	0.41 (0.11)	1.07 (0.15)	0.43 (0.14)
29	1.18 (0.22)	0.46 (0.17)	1.14 (0.14)	0.47 (0.11)	1.15 (0.17)	0.47 (0.13)	1.1 (0.16)	0.49 (0.15)
32	1.21 (0.24)	0.47 (0.18)	1.17 (0.15)	0.49 (0.12)	1.18 (0.18)	0.48 (0.13)	1.12 (0.17)	0.53 (0.17)
37	1.24 (0.26)	0.56 (0.21)	1.19 (0.16)	0.57 (0.15)	1.21 (0.19)	0.57 (0.16)	1.14 (0.17)	0.62 (0.2)
44	1.29 (0.27)	0.61 (0.23)	1.26 (0.17)	0.6 (0.16)	1.27 (0.21)	0.6 (0.17)	1.18 (0.18)	0.67 (0.22)
57	1.23 (0.33)	0.85 (0.28)	1.21 (0.19)	0.72 (0.19)	1.24 (0.23)	0.73 (0.22)	1.14 (0.21)	0.83 (0.3)
73	1.15 (0.39)	1.11 (0.35)	1.13 (0.21)	0.89 (0.26)	1.17 (0.25)	0.9 (0.28)	1.09 (0.25)	1.02 (0.38)
87	1.1 (0.45)	1.7 (0.44)	1.1 (0.24)	1.1 (0.36)	1.15 (0.28)	1.08 (0.35)	1.06 (0.28)	1.24 (0.47)
100.5	1.07 (0.48)	2.67 (0.57)	1.1 (0.27)	1.3 (0.47)	1.15 (0.31)	1.27 (0.45)	1.07 (0.31)	1.39 (0.54)

Formatted Table

Table 1A: Seasonal averages of tower sonic values of σ_w/u_* and T_L (for all sonic anemometer measurement heights on the Norunda flux tower) for the seasonal periods presented in Figure 6. Values shown are the mean with standard deviation in parentheses.

625

Figure 1A:

The level of coupling between the Norunda forest canopy and atmospheric boundary layer was also investigated using the decoupling factor Ω as described in Goldberg and Bernhofer (2001). The decoupling factor Ω is given by

630

$$\Omega = \frac{s + \gamma}{s + \gamma\left(1 + \frac{r_s}{r_a}\right)},$$ (A1)

where s is the slope of the saturation vapor pressure curve (Pa K^{-1}), γ is the psychrometric constant (Pa K^{-1}), r_a is the aerodynamic resistance, and r_s is the canopy resistance.

635

The decoupling factor Ω can range from 0 to 1. It quantifies the link between conditions at the canopy surface to the above-canopy atmosphere. Ω-values near to 0 indicate aerodynamically well-coupled conditions. This is characterized by strong transpiration control by stomatal resistance and the vapour pressure deficit between the canopy surface and the atmosphere. Ω-values near to 1 indicate aerodynamically decoupled conditions. In this case, transpiration is largely controlled by the

640 available energy (Jarvis and Mcnaughton, 1986).

In Goldberg and Bernhofer (2001), the resistances r_a and r_s are estimated based on the assumption that the heat transport only depends on aerodynamic resistance, and that the moisture transport only depends on canopy and aerodynamic resistance. Based on this, Goldberg and Bernhofer (2001) estimate that

645

$$r_a = \rho c_p (T_0 - T)/H$$ (A2)

and

$$r_s = \rho L(q_s(T_0) - q)/LE - r_a,$$ (A3)

650 where ρ is the air density (kg m^{-3}), c_p and L are the specific heat capacity of dry air (J K-1 kg-1) and latent heat of vaporisation (J Kg^{-1}). The values T_0 and $q_s(T_0)$ are the temperature (°C) and the specific saturation humidity (g Kg^{-1}), respectively, of the active canopy surface (in this case for this 2014-2016 campaign period, the canopy height was at 28 m height for the Norunda forest). Meanwhile, T and q are the temperature (°C) and the specific humidity (g Kg^{-1}), respectively, of the chosen atmospheric reference layer above the forest canopy (in this case, it was chosen to be at 57 m on the Norunda

655 flux tower). The values H and LE represent the sensible heat flux (W m^{-2}) and latent heat flux (W m^{-2}), respectively, between the canopy surface and the chosen reference layer above the canopy.

For the campaign, Ω typically varied between 0.1 and 0.6. The nighttime-daytime transition did appear to have an influence on the coupling, with peaks in the decoupling factor occurring at sunrise and sunset times. Regarding seasonal dependence,
660 there tended to be more decoupling during spring and fall seasons than in the summer. An example of the estimated decoupling factors for several seasons is shown below.
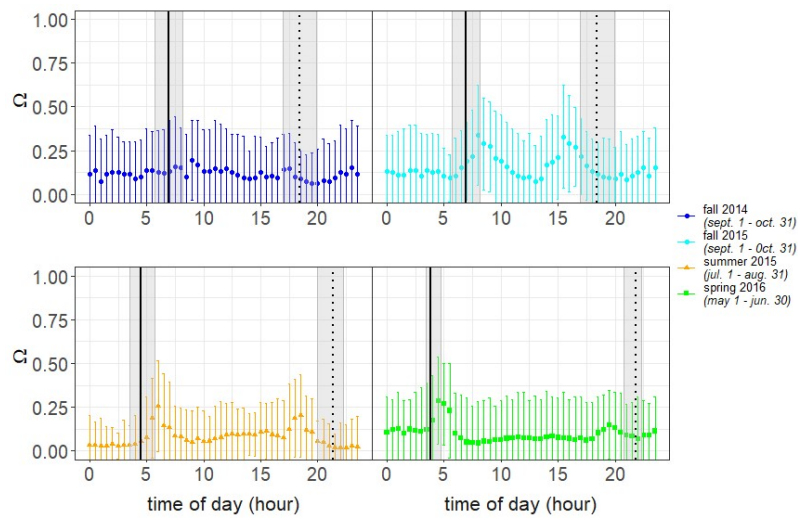
Figure 1A: Diurnal behaviour of the decoupling factor Ω for the seasonal periods presented in Figure 6. Points show the 30min average and error bars indicate the standard deviation.

665

Code and data availability

Station atmospheric and ecosystem data from the ICOS Norunda station is publicly available at https://www.icos-
670 sweden.se/norunda. The campaign data and scripts are available from the authors upon request.

Author contributions

JR, RCP, and TH initiated the study. JR and TH supervised the study and acquired the primary funding to support this research. RCP conducted the main study analysis and prepared the manuscript and figures, with contributions from JR, TH, MM, and NK. TH provided the PTR-MS and ozone data from the 2014 – 2016 campaign at ICOS Norunda. NK provided airborne LiDAR mapping data of tree height and assistance in estimating flux footprint climatology for the campaign period using the FFP footprint model (Kljun et al. 2015). MM provided the sonic anemometer data from the collection on the Norunda flux tower and technical feedback on the Lagrangian inversion analysis. All authors contributed to scientific discussion and revising the manuscript.

Competing interests

The authors declare that they have no conflict of interest.

Acknowledgements

This work was supported by the Swedish Research Councils VR (2011-3190) and Formas (2017-01474). The Norunda research station received funding by the Swedish Research Council VR, Grant 2019-00205. Airborne LiDAR for the Norunda site was acquired by Natascha Kljun with support from the British Natural Environment Research Council (NERC/ARSF/FSF grant EU10-01). We would like to thank the staff, A. Båth and I. Lehner, at the ICOS Norunda (SE-Nor) research station for their help and support.

References

Aalto, J., Kolari, P., Hari, P., Kerminen, V.-M., Schiestl-Aalto, P., Aaltonen, H., Levula, J., Siivola, E., Kulmala, M., and Bäck, J.: New foliage growth is a significant, unaccounted source for volatiles in boreal evergreen forests, Biogeosciences, 11, 1331-1344, 2014.

Aaltonen, H., Pumpanen, J., Pihlatie, M., Hakola, H., Hellén, H., Kulmala, L., Vesala, T., and Bäck, J.: Boreal pine forest floor biogenic volatile organic compound emissions peak in early summer and autumn, Agr. Forest Met., 151, 682-691, 2011.

Amin, H., Atkins, P. T., Russo, R. S., Brown, A. W., Sive, B., Hallar, A. G., and Huff Hartz, K. E.: Effect of bark beetle infestation on secondary organic aerosol precursor emissions, Environ. Sci. Technol., 46, 5696-5703, 2012.

Andreae, M. O. and Crutzen, P. J.: Atmospheric aerosols: Biogeochemical sources and role in atmospheric chemistry, Science, 276, 1052-1058, 1997.

Arneth, A., Schurgers, G., Lathiere, J., Duhl, T., Beerling, D., Hewitt, C., Martin, M., and Guenther, A.: Global terrestrial isoprene emission models: sensitivity to variability in climate and vegetation, Atmos. Chem. Phys., 11, 8037-8052, 2011.

Aubinet, M., Feigenwinter, C., Heinesch, B., Laffineur, Q., Papale, D., Reichstein, M., Rinne, J., and Gorsel, E. V.: Nighttime flux correction, in: Eddy covariance, Springer, 133-157, 2012.

Bäck, J., Aalto, J., Henriksson, M., Hakola, H., He, Q., and Boy, M.: Chemodiversity of a Scots pine stand and implications for terpene air concentrations, Biogeosciences, 9, 689-702, 2012.

Chameides, W., Fehsenfeld, F., Rodgers, M., Cardelino, C., Martinez, J., Parrish, D., Lonneman, W., Lawson, D.,
705 Rasmussen, R., and Zimmerman, P.: Ozone precursor relationships in the ambient atmosphere, J. Geophys. Res. Atmos., 97, 6037-6055, 1992.

Chameides, W. L.: Acid dew and the role of chemistry in the dry deposition of reactive gases to wetted surfaces, J. Geophys. Res. Atmos., 92, 11895-11908, 1987.

Cleveland, W., Grosse, E., and Shyu, W.: Local regression models. Chapter 8 in Statistical models in S (JM Chambers and
710 TJ Hastie eds.), 608 p, Wadsworth & Brooks/Cole, Pacific Grove, CA, 1992.

Cojocariu, C., Kreuzwieser, J., and Rennenberg, H.: Correlation of short-chained carbonyls emitted from Picea abies with physiological and environmental parameters, New Phytol., 162, 717-727, 2004.

Collins, W., Derwent, R., Johnson, C., and Stevenson, D.: The oxidation of organic compounds in the troposphere and their global warming potentials, Climatic Change, 52, 453-479, 2002.

715 Copolovici, L. O. and Niinemets, Ü.: Temperature dependencies of Henry's law constants and octanol/water partition coefficients for key plant volatile monoterpenoids, Chemosphere, 61, 1390-1400, 2005.

FAO: Global Forest Resources Assessment 2020, Rome, Italy, 184, https://doi.org/10.4060/ca8753en, 2020.

Fehsenfeld, F., Calvert, J., Fall, R., Goldan, P., Guenther, A. B., Hewitt, C. N., Lamb, B., Liu, S., Trainer, M., and Westberg, H.: Emissions of volatile organic compounds from vegetation and the implications for atmospheric chemistry, Global
720 Biogeochem. Cy., 6, 389-430, 1992.

Galbally, I. E. and Kirstine, W.: The production of methanol by flowering plants and the global cycle of methanol, J. Atmos. Chem., 43, 195-229, 2002.

Ghirardo, A., Koch, K., Taipale, R., Zimmer, I., SCHNITZLER, J. P., and Rinne, J.: Determination of de novo and pool emissions of terpenes from four common boreal/alpine trees by 13CO2 labelling and PTR-MS analysis, Plant Cell Environ.,
725 33, 781-792, 2010.

Goldberg, V. and Bernhofer, C.: Quantifying the coupling degree between land surface and the atmospheric boundary layer with the coupled vegetation-atmosphere model HIRVAC, Ann. Geophys., 581-587,

Guenther, A., Hewitt, C. N., Erickson, D., Fall, R., Geron, C., Graedel, T., Harley, P., Klinger, L., Lerdau, M., and McKay, W.: A global model of natural volatile organic compound emissions, J. Geophys. Res., 100, 8873-8892, 1995.

730 Guenther, A. B., Zimmerman, P. R., Harley, P. C., Monson, R. K., and Fall, R.: Isoprene and monoterpene emission rate variability: model evaluations and sensitivity analyses, J. Geophys. Res. Atmos., 98, 12609-12617, 1993.

Hakola, H., Tarvainen, V., Praplan, A. P., Jaars, K., Hemmilä, M., Kulmala, M., Bäck, J., and Hellén, H.: Terpenoid and carbonyl emissions from Norway spruce in Finland during the growing season, Atmos. Chem. Phys., 17, 3357-3370, 2017.

Holst, T., Arneth, A., Hayward, S., Ekberg, A., Mastepanov, M., Jackowicz-Korczynski, M., Friborg, T., Crill, P. M., and
735 Bäckstrand, K.: BVOC ecosystem flux measurements at a high latitude wetland site, Atmos. Chem. Phys., 10, 1617-1634, 2010.

Hüve, K., Christ, M., Kleist, E., Uerlings, R., Niinemets, Ü., Walter, A., and Wildt, J.: Simultaneous growth and emission measurements demonstrate an interactive control of methanol release by leaf expansion and stomata, J. Exp. Bot., 58, 1783-1793, 2007.

740 Jardine, K. J., Sommer, E. D., Saleska, S. R., Huxman, T. E., Harley, P. C., and Abrell, L.: Gas phase measurements of pyruvic acid and its volatile metabolites, Environ. Sci. Technol., 44, 2454-2460, 2010.

Jarvis, P. G. and McNaughton, K.: Stomatal control of transpiration: scaling up from leaf to region, in: Adv. Ecol. Res., Elsevier, 1-49, 1986.

Kainulainen, P. and Holopainen, J.: Concentrations of secondary compounds in Scots pine needles at different stages of
745 decomposition, Soil Biol. Biochem., 34, 37-42, 2002.

Karl, T., Curtis, A., Rosenstiel, T., Monson, R., and Fall, R.: Transient releases of acetaldehyde from tree leaves− products of a pyruvate overflow mechanism?, Plant Cell Environ., 25, 1121-1131, 2002.

Karl, T., Potosnak, M., Guenther, A., Clark, D., Walker, J., Herrick, J. D., and Geron, C.: Exchange processes of volatile organic compounds above a tropical rain forest: Implications for modeling tropospheric chemistry above dense vegetation, J.
750 Geophys. Res. Atmos., 109, 2004.

Kljun, N., Calanca, P., Rotach, M., and Schmid, H. P.: A simple two-dimensional parameterisation for Flux Footprint Prediction (FFP), Geosci. Instrum. Dev., 8, 3695-3713, 2015.

Kreuzwieser, J., Scheerer, U., and Rennenberg, H.: Metabolic origin of acetaldehyde emitted by poplar (Populus tremula× P. alba) trees, J. Exp. Bot., 50, 757-765, 1999.

755 Kreuzwieser, J., Kühnemann, F., Martis, A., Rennenberg, H., and Urban, W.: Diurnal pattern of acetaldehyde emission by flooded poplar trees, Physiol. Plant., 108, 79-86, 2000.

Lagergren, F., Eklundh, L., Grelle, A., Lundblad, M., Mölder, M., Lankreijer, H., and Lindroth, A.: Net primary production and light use efficiency in a mixed coniferous forest in Sweden, Plant Cell Environ., 28, 412-423, 2005.

Liedvogel, B. and Stumpf, P. K.: Origin of acetate in spinach leaf cell, Plant Physiol., 69, 897-903, 1982.

760 Lindfors, V. and Laurila, T.: Biogenic volatile organic compound (VOC) emissions from forests in Finland, Boreal Environ. Res., 5, 95-113, 2000.

Lindinger, W., Hansel, A., and Jordan, A.: On-line monitoring of volatile organic compounds at pptv levels by means of proton-transfer-reaction mass spectrometry (PTR-MS) medical applications, food control and environmental research, Int. J. Mass Spectrom. Ion Proc., 173, 191-241, 1998.

765 Lindroth, A., Grelle, A., and Morén, A. S.: Long-term measurements of boreal forest carbon balance reveal large temperature sensitivity, Global Change Biol., 4, 443-450, 1998.

Loreto, F. and Schnitzler, J.-P.: Abiotic stresses and induced BVOCs, Trends Plant Sci., 15, 154-166, 2010.

Lundin, L.-C., Halldin, S., Lindroth, A., Cienciala, E., Grelle, A., Hjelm, P., Kellner, E., Lundberg, A., Mölder, M., and Morén, A.-S.: Continuous long-term measurements of soil-plant-atmosphere variables at a forest site, Agr. Forest Met., 98, 770 53-73, 1999.

Macdonald, R. C. and Fall, R.: Acetone emission from conifer buds, Phytochemistry, 34, 991-994, 1993a.

MacDonald, R. C. and Fall, R.: Detection of substantial emissions of methanol from plants to the atmosphere, Atmos. Environ., 27, 1709-1713, 1993b.

Mäki, M., Aalto, J., Hellén, H., Pihlatie, M., and Bäck, J.: Interannual and seasonal dynamics of volatile organic compound 775 fluxes from the boreal forest floor, Front. Plant Sci., 10, 191, 2019a.

Mäki, M., Aaltonen, H., Heinonsalo, J., Hellén, H., Pumpanen, J., and Bäck, J.: Boreal forest soil is a significant and diverse source of volatile organic compounds, Plant Soil, 441, 89-110, 2019b.

McKeen, S., Gierczak, T., Burkholder, J., Wennberg, P., Hanisco, T., Keim, E., Gao, R. S., Liu, S., Ravishankara, A., and Fahey, D.: The photochemistry of acetone in the upper troposphere: A source of odd-hydrogen radicals, Geophys. Res. Lett., 780 24, 3177-3180, 1997.

Menke, W.: Geophysical data analysis: Discrete inverse theory, Elsevier, Amsterdam2018.

Mölder, M., Klemedtsson, L., and Lindroth, A.: Turbulence characteristics and dispersion in a forest—tests of Thomson's random-flight model, Agr. Forest Met., 127, 203-222, 2004.

Nemitz, E., Sutton, M. A., Gut, A., San José, R., Husted, S., and Schjoerring, J. K.: Sources and sinks of ammonia within an 785 oilseed rape canopy, Agr. Forest Met., 105, 385-404, 2000.

Niinemets, Ü.: Mild versus severe stress and BVOCs: thresholds, priming and consequences, Trends Plant Sci., 15, 145-153, 2010.

Niinemets, Ü. and Monson, R. K.: Biology, controls and models of tree volatile organic compound emissions, Springer2013.

Niinemets, Ü. and Reichstein, M.: Controls on the emission of plant volatiles through stomata: Differential sensitivity of 790 emission rates to stomatal closure explained, J. Geophys. Res. Atmos., 108, 2003.

Noe, S., Copolovici, L., Niinemets, Ü., and Vaino, E.: Foliar limonene uptake scales positively with leaf lipid content:"non-emitting" species absorb and release monoterpenes, Plant Biol., 9, e79-e86, 2007.

Ouwersloot, H., Vilà-Guerau de Arellano, J., Nölscher, A., Krol, M., Ganzeveld, L., Breitenberger, C., Mammarella, I., Williams, J., and Lelieveld, J.: Characterization of a boreal convective boundary layer and its impact on atmospheric 795 chemistry during HUMPPA-COPEC-2010, Atmos. Chem. Phys., 12, 9335-9353, 2012.

Paasonen, P., Asmi, A., Petäjä, T., Kajos, M. K., Äijälä, M., Junninen, H., Holst, T., Abbatt, J. P., Arneth, A., and Birmili, W.: Warming-induced increase in aerosol number concentration likely to moderate climate change, Nature Geoscience, 6, 438-442, 2013.

Rantala, P., Aalto, J., Taipale, R., Ruuskanen, T., and Rinne, J.: Annual cycle of volatile organic compound exchange 800 between a boreal pine forest and the atmosphere, Biogeosciences, 12, 5753-5770, 2015.

Rantala, P., Taipale, R., Aalto, J., Kajos, M. K., Patokoski, J., Ruuskanen, T. M., and Rinne, J.: Continuous flux measurements of VOCs using PTR-MS—reliability and feasibility of disjunct-eddy-covariance, surface-layer-gradient, and surface-layer-profile methods, Boreal Environ. Res., 19, 87-107, 2014.

Raupach, M.: Applying Lagrangian fluid mechanics to infer scalar source distributions from concentration profiles in plant canopies, Agr. Forest Met., 47, 85-108, 1989.

Raupach, M., Coppin, P., and Legg, B.: Experiments on scalar dispersion within a model plant canopy part I: The turbulence structure, Boundary Layer Meteorol., 35, 21-52, 1986.

Rebmann, C., Aubinet, M., Schmid, H., Arriga, N., Aurela, M., Burba, G., Clement, R., De Ligne, A., Fratini, G., and Gielen, B.: ICOS eddy covariance flux-station site setup: a review, Int. Agrophys., 32, 471-494, 2018.

Rinne, J., Bäck, J., and Hakola, H.: Biogenic volatile organic compound emissions from the Eurasian taiga: current knowledge and future directions, Boreal Environ. Res., 14, 2009.

Rinne, J., Ruuskanen, T. M., Reissell, A., Taipale, R., Hakola, H., and Kulmala, M.: On-line PTR-MS measurements of atmospheric concentrations of volatile organic compounds in a European boreal forest ecosystem, Boreal Environ. Res., 10, 425-436, 2005.

Rinne, J., Taipale, R., Markkanen, T., Ruuskanen, T. M., Hellén, H., Kajos, M., Vesala, T., and Kulmala, M.: Hydrocarbon fluxes above a Scots pine forest canopy: measurements and modeling, Atmos. Chem. Phys., 7, 3361-3372, 2007.

Rinne, J., Markkanen, T., Ruuskanen, T., Petäjä, T., Keronen, P., Tang, M., Crowley, J., Rannik, Ü., and Vesala, T.: Effect of chemical degradation on fluxes of reactive compounds–a study with a stochastic Lagrangian transport model, Atmos. Chem. Phys., 12, 4843-4854, 2012.

Roberts, J. M., Flocke, F., Stroud, C. A., Hereid, D., Williams, E., Fehsenfeld, F., Brune, W., Martinez, M., and Harder, H.: Ground-based measurements of peroxycarboxylic nitric anhydrides (PANs) during the 1999 Southern Oxidants Study Nashville Intensive, J. Geophys. Res. Atmos., 107, ACH 1-1-ACH 1-10, 2002.

Roldin, P., Ehn, M., Kurtén, T., Olenius, T., Rissanen, M. P., Sarnela, N., Elm, J., Rantala, P., Hao, L., and Hyttinen, N.: The role of highly oxygenated organic molecules in the Boreal aerosol-cloud-climate system, Nature communications, 10, 4370, 2019.

Ruuskanen, T., Taipale, R., Rinne, J., Kajos, M., Hakola, H., and Kulmala, M.: Quantitative long-term measurements of VOC concentrations by PTR-MS: annual cycle at a boreal forest site, Atmos. Chem. Phys. Disc., 9, 81-134, 2009.

Schade, G. W. and Goldstein, A. H.: Increase of monoterpene emissions from a pine plantation as a result of mechanical disturbances, Geophys. Res. Lett., 30, 2003.

Schurgers, G., Arneth, A., Holzinger, R., and Goldstein, A.: Process-based modelling of biogenic monoterpene emissions combining production and release from storage, Atmos. Chem. Phys., 9, 3409-3423, 2009.

Seco, R., Penuelas, J., and Filella, I.: Short-chain oxygenated VOCs: Emission and uptake by plants and atmospheric sources, sinks, and concentrations, Atmos. Environ., 41, 2477-2499, 2007.

Seinfeld, J. H. and Pandis, S. N.: Atmospheric chemistry and physics: from air pollution to climate change, John Wiley & Sons2016.

Simpson, D., Winiwarter, W., Börjesson, G., Cinderby, S., Ferreiro, A., Guenther, A., Hewitt, C. N., Janson, R., Khalil, M. A. K., and Owen, S.: Inventorying emissions from nature in Europe, J. Geophys. Res. Atmos., 104, 8113-8152, 1999.

Siqueira, M., Katul, G., and Lai, C.-T.: Quantifying net ecosystem exchange by multilevel ecophysiological and turbulent transport models, AdWR, 25, 1357-1366, 2002.

Siqueira, M., Lai, C. T., and Katul, G.: Estimating scalar sources, sinks, and fluxes in a forest canopy using Lagrangian, Eulerian, and hybrid inverse models, J. Geophys. Res. Atmos., 105, 29475-29488, 2000.

Siqueira, M., Leuning, R., Kolle, O., Kelliher, F., and Katul, G.: Modelling sources and sinks of CO2, H2O and heat within a Siberian pine forest using three inverse methods, Quarterly Journal of the Royal Meteorological Society: A journal of the atmospheric sciences, applied meteorology and physical oceanography, 129, 1373-1393, 2003.

Steinbacher, M., Dommen, J., Ammann, C., Spirig, C., Neftel, A., and Prevot, A.: Performance characteristics of a proton-transfer-reaction mass spectrometer (PTR-MS) derived from laboratory and field measurements, Int. J. Mass spectrom., 239, 117-128, 2004.

Taipale, R., Kajos, M. K., Patokoski, J., Rantala, P., Ruuskanen, T. M., and Rinne, J.: Role of de novo biosynthesis in ecosystem scale monoterpene emissions from a boreal Scots pine forest, Biogeosciences, 8, 2247-2255, 2011.

850   Tani, A., Hayward, S., and Hewitt, C.: Measurement of monoterpenes and related compounds by proton transfer reaction-mass spectrometry (PTR-MS), Int. J. Mass spectrom., 223, 561-578, 2003.

Tarvainen, V., Hakola, H., Rinne, J., HellàN, H., and Haapanala, S.: Towards a comprehensive emission inventory of terpenoids from boreal ecosystems, Tellus B: Chemical and Physical Meteorology, 59, 526-534, 2007.

Thomsen, D., Elm, J., Rosati, B., Skønager, J. T., Bilde, M., and Glasius, M.: Large discrepancy in the formation of
855   secondary organic aerosols from structurally similar monoterpenes, ACS Earth and Space Chemistry, 5, 632-644, 2021.

Tingey, D. T., Manning, M., Grothaus, L. C., and Burns, W. F.: Influence of light and temperature on monoterpene emission rates from slash pine, Plant Physiol., 65, 797-801, 1980.

Vilà-Guerau de Arellano, J., Van den Dries, K., and Pino, D.: On inferring isoprene emission surface flux from atmospheric boundary layer concentration measurements, Atmos. Chem. Phys., 9, 3629-3640, 2009.

860   Wang, M., Schurgers, G., Arneth, A., Ekberg, A., and Holst, T.: Seasonal variation in biogenic volatile organic compound (BVOC) emissions from Norway spruce in a Swedish boreal forest, Boreal Environ. Res., 22, 353-367, 2017.

Wang, M., Schurgers, G., Hellén, H., Lagergren, F., and Holst, T.: Biogenic volatile organic compound emissions from a boreal forest floor, Boreal Environ. Res., 23, 249-265, 2018.

Warland, J. S. and Thurtell, G. W.: A Lagrangian solution to the relationship between a distributed source and concentration
865   profile, Boundary Layer Meteorol., 96, 453-471, 2000.

Wilson, J. D. and Flesch, T. K.: Flow boundaries in random-flight dispersion models: enforcing the well-mixed condition, Journal of Applied Meteorology and Climatology, 32, 1695-1707, 1993.

Wohlfahrt, G., Amelynck, C., Ammann, C., Arneth, A., Bamberger, I., Goldstein, A. H., Gu, L., Guenther, A., Hansel, A., and Heinesch, B.: An ecosystem-scale perspective of the net land methanol flux: synthesis of micrometeorological flux
870   measurements, Atmos. Chem. Phys., 15, 7413-7427, 2015.

Zhou, P., Ganzeveld, L., Taipale, D., Rannik, Ü., Rantala, P., Rissanen, M. P., Chen, D., and Boy, M.: Boreal forest BVOC exchange: emissions versus in-canopy sinks, Atmos. Chem. Phys., 17, 14309-14332, 2017.